

Research article

## Fine-scale analysis of the cumulative and time-lagged effects of drought on vegetation in the Ili River Basin, Central Asia



Mengzhen Huang <sup>a,b</sup>, Ruijie Lu <sup>a,b,\*</sup> , Zhiyong Zhang <sup>c</sup>, Yue Zhou <sup>a,b</sup>, Peiru Li <sup>a,b</sup>, Peng Du <sup>c</sup>, Tian Zhao <sup>c</sup>, Sining Xiao <sup>c</sup>

<sup>a</sup> Engineering Center of Desertification and Blown-Sand Control of Ministry of Education, Faculty of Geographical Science, Beijing Normal University, Beijing, 100875, China

<sup>b</sup> State Key Laboratory of Earth Surface Processes and Disaster Risk Reduction, Faculty of Geographical Science, Beijing Normal University, Beijing, 100875, China

<sup>c</sup> Xinjiang Uygur Autonomous Region Natural Disaster Comprehensive Monitoring and Early Warning Center, Xinjiang Uygur Autonomous Region, Urumqi, 830000, China

ARTICLE INFO

**Keywords:**

Time-lagged effects  
Cumulative effects  
Gross primary productivity  
Standardized precipitation evapotranspiration index  
Carbon cycle

ABSTRACT

Under intensifying climate change, drought impacts on vegetation have become increasingly complex. Although the Ili River Basin is highly sensitive to drought, the underlying mechanisms of drought–vegetation interactions remain insufficiently understood. This study quantifies the cumulative, time-lagged, and dominant effects of drought on vegetation gross primary productivity (GPP) at the daily scale, and investigates their variations across land use types, wetness gradients, and seasons. Fine-scale ecosystem management strategies are further proposed, tailored to both land use and seasonal conditions. The findings are: (1) Over the past 40 years, growing season GPP increased ( $k = 1.302 \text{ C/m}^2/\text{a}$ ), while drought conditions intensified ( $k = -0.002/\text{a}$ ). (2) Cumulative drought effects suppressed GPP in over 90 % of the basin, with accumulation durations concentrated around 180 and 90 days. Cumulative effects intensified and extended with increasing drought severity. (3) Time-lagged effects exhibited spatial heterogeneity, with 58 % of the basin showing post-drought GPP promotion after 280 days and 42 % showing suppression after 117 days. Time-lagged effects also strengthened with drought intensity. (4) Positive cumulative effects dominated 77 % of the basin, with their spatial extent increasing under more severe drought. (5) Seasonally, spring exhibited strong lagged suppression but low sensitivity, summer showed the strongest and most sensitive cumulative suppression, while autumn displayed signs of compensatory recovery. Among land use types, grassland exhibited the highest sensitivity to drought. Differentiated management strategies should be adopted by season and land use, with emphasis on enhancing drought monitoring and water regulation in spring and summer, and prioritizing drought risk prevention and adaptive management in grassland.

### 1. Introduction

Drought is a persistent water shortage phenomenon caused by an imbalance between regional water supply and demand (Mishra and Singh, 2010). As one of the most prevalent natural disasters globally, it is characterized by long duration and widespread impact (Wilhite, 2016). With the intensification of global warming, the frequency and intensity of drought events continue to increase, expanding their scope of impact (Zhang et al., 2022a). In arid and semi-arid regions with fragile ecosystems, drought significantly affects vegetation (Wu et al., 2022; Liu et al., 2021b; Luo et al., 2020), leading to slowed growth, decreased

productivity, and increased mortality rates (van der Molen et al., 2011; Xu et al., 2019). Therefore, investigating the mechanisms of drought impacts on vegetation in arid and semi-arid regions is of both scientific and practical significance for maintaining global carbon balance and addressing the potential challenges of climate change.

Soil moisture plays a central role in regulating vegetation growth under drought conditions, yet its response to meteorological drought often exhibits a temporal lag (Xu et al., 2023). Consequently, vegetation is influenced not only by contemporaneous water availability but also by antecedent deficits in soil moisture. In parallel, plants have evolved a suite of adaptive mechanisms to mitigate drought-induced stress,

\* Corresponding author. Faculty of Geographical Sciences, Beijing Normal University, No. 19, Xinjiekouwai Street, Haidian District, Beijing, 100875, China.  
E-mail address: ruijielu@bnu.edu.cn (R. Lu).

including modifications in root architecture, stomatal regulation, leaf morphology, and post-drought remobilization of stored carbon and nutrients (Liu et al., 2023b; Zhang et al., 2018a). These physiological and hydrological processes jointly contribute to non-instantaneous vegetation responses, manifesting as time-lagged and cumulative effects (Zhao et al., 2020). The time-lagged effect denotes the delayed influence of climatic anomalies at a specific prior time on current vegetation productivity (Braswell et al., 1997), whereas the cumulative effect reflects the integrated impact of sustained climatic stress over a preceding period (Wen et al., 2019).

Recent studies have confirmed the widespread presence of drought-induced cumulative effects on gross primary productivity (GPP), with a global average accumulation period of approximately 4.89 months (Zhang et al., 2022b). These effects vary depending on vegetation type and climatic conditions. This variation is largely attributed to differences in plant structural and functional traits, including rooting depth, leaf area index, and water use efficiency (Comas et al., 2013; Lozano et al., 2020). Additionally, spatial heterogeneity in water availability further influences the manifestation of drought responses (Peng et al., 2019). At the regional scale, Zhao et al. (2020) found that grasslands on the Chinese Loess Plateau exhibit cumulative effects over 5–10 months and time-lagged effects over 2–3 months. Based on Standardized Precipitation Evapotranspiration Index (SPEI) and Net Primary Productivity (NPP), Liu et al. (2023a, 2023b) reported that cumulative and lagged effects influenced 30.02 % and 69.98 % of the region, with average durations of 6.72 and 5.36 months, respectively; lagged responses exhibited a nonlinear relationship with water availability. In contrast, Lu et al. (2023) using SPEI and GPP, found more extensive impacts, with 95.6 % and 95.8 % of grasslands affected by lagged (2–3 months) and cumulative effects (4, 5, and 10 months), respectively. They further identified a linear relationship between SPEI gradients and drought effects. Despite these findings, substantial inconsistencies persist among studies conducted at different spatial scales. These discrepancies may stem from variations in drought characteristics, vegetation types, soil properties, and anthropogenic influences (Sheffield and Wood, 2007). Even within the same region, differences in the selection of drought indices or vegetation metrics can lead to divergent conclusions (Li et al., 2023). Among various drought indices, the SPEI, which includes both precipitation and evapotranspiration, works across multiple time scales and effectively captures cumulative drought effects (Tirivarombo et al., 2018). Vegetation responses are typically assessed using indicators such as GPP, NPP, and NDVI. GPP, representing total photosynthetic carbon fixation by photosynthesis (Anav et al., 2015), is a key indicator of the terrestrial carbon cycle and exhibits greater drought sensitivity (Wu et al., 2022). Therefore, it is essential to conduct fine-scale assessments at regional or watershed scale, where the appropriate selection of drought indicators and vegetation parameters can enhance the understanding of vegetation responses to drought.

The arid region of Central Asia is highly sensitive to climate change, with ecosystems strongly influenced by hydrothermal variability (Immerzeel et al., 2010). Recent studies have explored drought impacts on vegetation productivity (Liu et al., 2023a, 2023b; Lu et al., 2023; Jiang et al., 2024). However, three key limitations remain. First, most analyses are based on monthly or coarser data due to limited temporal resolution, making it difficult to capture rapid vegetation responses or support timely decision-making for agricultural and pastoral management and disaster mitigation. Second, existing studies predominantly focus on grasslands, which cover over 60 % of the Central Asian region, while lacking systematic comparisons across other land use types. However, different vegetation types exhibit distinct sensitivities and adaptive strategies to drought (Comas et al., 2013; Lozano et al., 2020), highlighting the need for a more comprehensive perspective that incorporates diverse land-use types. Third, strong spatial heterogeneity exists in drought–vegetation relationships. While most grassland areas in Central Asia show positive correlations between drought and productivity, the region surrounding Lake Balkhash shows significant

negative correlations (Liu et al., 2023a, 2023b; Lu et al., 2023). These studies commonly use the maximum correlation coefficient to assess drought effects, which performs well in positively correlated regions but may underestimate the response intensity and misrepresent the direction in negatively correlated areas, resulting in an incomplete understanding of ecological dynamics.

These challenges are particularly evident in the Ili River Basin (IRB), located in the interior of Central Asia. The region experiences highly uneven spatiotemporal precipitation, frequent droughts, and a fragile ecological environment (Lioubimtseva and Henebry, 2009). Grasslands dominate land use, covering approximately 87 % of the area, alongside croplands and bare lands. Together, these form a transitional ecological zone extending from mountain snowpacks to riverine oases and desert grasslands (Liang et al., 2020). As one of the best-preserved semi-arid ecological landscapes globally, the IRB has increasingly drawn scholarly attention for its ecological significance and vulnerability. Recent studies have investigated vegetation vulnerability to drought stress in the IRB (Li et al., 2025; Yu et al., 2023), but most have concentrated on concurrent drought–vegetation relationships, with limited attention to cumulative and time-lagged effects. In addition, spatial heterogeneity in vegetation responses across land-use types and wetness gradients remains poorly understood. Given the IRB's ecological significance and representativeness, fine-scale assessments of the cumulative and time-lagged impacts of drought on vegetation productivity are crucial.

Building on the above research background, this study aims to: (1) characterize the spatiotemporal characteristics of GPP and drought in the IRB; (2) integrate high-resolution daily GPP and multi-scale SPEI to construct a continuous 0–365 days lag window, and assess the cumulative, time-lagged and dominant effects of drought in terms of their intensity, duration, and direction (suppress or promote); (3) explore the heterogeneity of drought effects across different land use types and wetness gradients, and propose fine-scale ecosystem management strategies from the perspectives of both seasonality and land use. The findings are expected to enhance understanding of ecosystem carbon dynamics under climate change and provide scientific support for drought mitigation and adaptive strategies in agriculture and livestock management.

## 2. Materials and methods

### 2.1. Study area

The IRB ( $72.00^{\circ}$ – $85.00^{\circ}$ E,  $42.26^{\circ}$ – $49.37^{\circ}$ N), located in the heart of Central Asia (Fig. 1a), is considered one of the best-preserved semi-arid ecological landscapes globally (Liang et al., 2020). Originating from the north side of the Tianshan Khantengri Peak within China, the Ili River flows westward into Kazakhstan and empties into Lake Balkhash (Xi et al., 2024). The total basin area is 151,000 km<sup>2</sup>, with 37 % (56,000 km<sup>2</sup>) in western Xinjiang, China, and 63 % (95,000 km<sup>2</sup>) in southeastern Kazakhstan. The IRB is characterized by a temperate continental climate. Based on the aridity index (Arora, 2002), the basin encompasses arid, semi-arid, semi-humid, and humid zones, of which arid and semi-arid areas together account for 92 % of the total area (Fig. 1b). Land use in the IRB includes grassland (covering 87 % of the area), cropland (5 %), bare land (2 %), and forests (0.37 %). Grasslands are mainly distributed across Kazakhstan and the mountainous regions of the Ili Kazakh Autonomous Prefecture in China. Croplands are concentrated in river valleys and the southwestern of the Ili Kazakh Autonomous Prefecture, with some scattered in the southeastern Almaty Region. Bare lands are primarily found in the northern and southern margins of the Ili Kazakh Autonomous Prefecture, along the mountain edges of southeastern Almaty Region, and near Lake Balkhash (Fig. 1c). This study focuses on grasslands, croplands, and bare lands as the principal land use types to evaluate vegetation responses to drought.

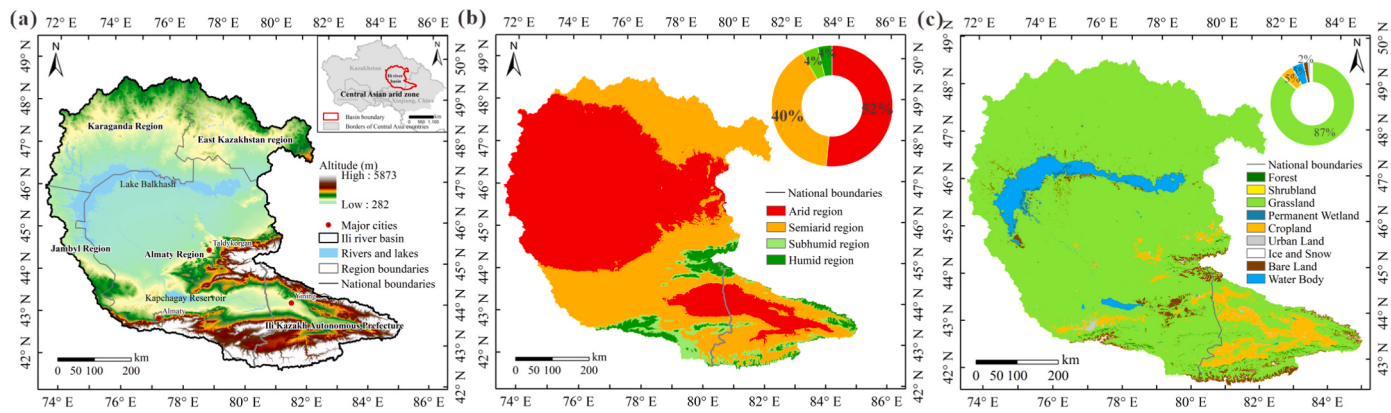


**Fig. 1.** Overview of the study area. (a) Location and elevation; (b) Climate zone distribution; (c) Land use types.

## 2.2. Data sources

The daily SPEI data used in this study is derived from the first global multi-timescale daily SPEI dataset (SPEI-GD), developed by Peking University (Liu et al., 2024). This dataset features a daily temporal resolution and a spatial resolution of  $0.25^\circ$ , and includes five timescales: 5, 30, 90, 180, and 360 days. Compared to the widely used SPEIbase dataset, SPEI-GD offers improved spatiotemporal resolution and enhanced accuracy, particularly in regions with sparse meteorological observations. Moreover, SPEI-GD shows strong correlations with station-based SPEI values and soil moisture, thereby providing a robust foundation for global and regional drought studies at sub-seasonal to daily scales. Liu et al. (2024) categorized the climate wet and dry conditions indicated by the SPEI into 9 classes, as detailed in Table A.1.

The daily GPP data used in this study is sourced from the global daily GPP simulation product developed by Nanjing University (GPP<sub>BEPS</sub>) (He et al., 2021). This dataset is generated using the Boreal Ecosystem Productivity Simulator (BEPS), a mechanistic ecological model, and provides a daily temporal resolution and a spatial resolution of  $0.072727^\circ$ . The dataset consists of daily accumulated GPP values, from which the actual daily GPP for day n was derived by subtracting the cumulative value of day n-1 from that of day n. Compared to the MODIS GPP dataset, which has an 8-day temporal resolution, this dataset offers significantly finer temporal granularity, thereby enabling high-precision analysis at the daily scale.

The land use data has a spatial resolution of 500 m and comes from the MODIS land cover classification product version 6 (MCD12Q1\_V06, <https://ladsweb.modaps.eosdis.nasa.gov/search/order/1/MCD12Q1-6>). The DEM data has a spatial resolution of 30 s and is sourced from GMTED2010 (<https://www.usgs.gov/coastal-changes-and-impacts/gmted2010>). Other basic geographic information data used in this study is shown in Table A.2.

This study analyzes vegetation response to drought during the growing season (April to October, corresponding to days 90–303 of the year) to effectively capture the relationship between drought and vegetation productivity. To ensure comparability across multiple datasets, the spatial resolution of the SPEI data was resampled to  $0.072727^\circ$  using bilinear interpolation.

To validate the accuracy of the SPEI-GD dataset used in this study, we employed SPEI data calculated by Wang et al. (2021), which is derived from daily meteorological observations at 427 stations across China. Specifically, we compared SPEI-GD at 30-, 90-, 180-, and 360-day time scales with station-based SPEI values computed at 1-, 3-, 6-, and 12-month time scales, respectively. Validation was conducted using data from two meteorological stations surrounding the IRB region, and the comparison results are summarized in Table A.3. Significant positive correlations ( $p < 0.05$ ) were found across all time scales, with the highest correlation (up to  $r = 0.6$ ) observed at the 360-day scale. To

assess the reliability of the GPP<sub>BEPS</sub> dataset adopted in this study, we performed a comparative analysis against three widely used annual GPP products: FluxSat M, GLASS, and MODIS. As shown in Fig. A.1 and Table A.4, the correlation coefficients between GPP<sub>BEPS</sub> and the other datasets all exceeded 0.7. Moreover, over 90 % of the IRB exhibited statistically significant correlations ( $p < 0.05$ ), indicating a high level of spatial agreement. These results confirm the high reliability of both the SPEI-GD and the GPP<sub>BEPS</sub> dataset in the IRB.

## 2.3. Methodology

### 2.3.1. Trend and abrupt analysis

Sen's slope analysis (Theil, 1950; Sen, 1968) was applied to quantify the overall trends of SPEI and GPP. This non-parametric method does not require the data to follow a specific distribution and is robust against outliers, making it effective for identifying monotonic trends in environmental datasets (Dawood, 2017). The method estimates the median of all possible pairwise slopes in the time series, which is then used to represent the overall trend. A positive Sen's slope indicates an increasing trend, whereas a negative value indicates a decreasing trend.

To assess the statistical significance of these trends, the Mann-Kendall (MK) test was employed. As a non-parametric statistical test, the MK method is not sensitive to missing values or outliers and is widely used in environmental time series analysis (Mann, 1945; Kendall, 1948). In this study, the MK trend test was used to evaluate the significance of trends in SPEI and GPP, while the MK abrupt test was used to detect possible shift points in their temporal variability. A significance level of 0.05 (corresponding to a critical value of  $\pm 1.96$ ) was adopted. If the forward (UF<sub>K</sub>) and backward (UB<sub>K</sub>) MK statistic curves intersect within the confidence interval, the corresponding time is identified as a potential change point (Mondal et al., 2012; Dhital et al., 2013).

### 2.3.2. Determination of the cumulative effects of drought

The SPEI at different time scales represents the climatic dry-wet conditions over varying accumulation periods (Drumond et al., 2021). For instance, SPEI-5 reflects dry-wet conditions accumulated over 5 days, and SPEI-360 over 360 days. We quantify the cumulative effects of drought on vegetation by calculating the Pearson correlation coefficient (R) between daily growing season GPP (1982–2019) and daily SPEI at various time scales (Wei et al., 2022). The R ranges from -1 to +1, indicating the direction and intensity of the relationship between drought and vegetation GPP (Table A.5). A positive correlation ( $R > 0$ ) indicates that increasing drought severity (decreasing SPEI) suppresses vegetation growth, resulting in lower GPP. Conversely, a negative correlation ( $R < 0$ ) suggests an increase in vegetation GPP under intensified drought, potentially due to lagged responses, adaptive traits, or confounding influences such as irrigation and land use (Ding et al., 2024). Regardless of the sign of the correlation, its absolute magnitude ( $|R|$ )

reflects the intensity of the relationship. Therefore, the correlation coefficient with the maximum absolute value was taken as the intensity of the cumulative effect, and the corresponding time scale as the accumulation duration (Peng et al., 2019). The analysis is performed as follows:

- (1) Correlate the GPP time series with SPEI time series at different scales ( $n = 5, 30, 90, 180, 360$  days), calculating the correlation coefficient  $R_n$  for each scale. Each pixel will yield five correlation coefficients corresponding to the time scales. (2) Identify the time scale of the maximum absolute correlation coefficient  $R_{max\_cum}$  as the cumulative effect's time scale and use  $R_{max\_cum}$  as the intensity of the cumulative effect.

$$R_n = \text{corr}(GPP, SPEI - n), n = 5, 30, 90, 180, 360 \quad (1)$$

$$R_{max\_cum} = \begin{cases} \max(R_n), |\max(R_n)| > |\min(R_n)| \\ \min(R_n), |\max(R_n)| < |\min(R_n)| \end{cases} \quad (2)$$

If  $R_{max\_cum} > 0$ , the result is classified as a positive cumulative effect (PCE), indicating that drought accumulation leads to a decline in GPP. Conversely, if  $R_{max\_cum} < 0$ , the effect is classified as a negative cumulative effect (NCE), implying that GPP increases following a period of drought accumulation.

### 2.3.3. Determination of the time-lagged effects of drought

To study the time-lagged effects of drought on vegetation GPP, a correlation analysis was conducted between the SPEI series and GPP series at different lag times (Wei et al., 2022). The SPEI-GD dataset includes five time-scales (5, 30, 90, 180, and 360 days). For consistency, the smallest scale, SPEI-5, was selected to represent daily dry-wet conditions for correlation analysis with growing season GPP (Liu et al., 2024). Like the cumulative effect analysis, the assessment of time-lagged effects also considers both the magnitude and direction of the correlation between SPEI and GPP across different lag days. Therefore, the correlation coefficient with the maximum absolute value was used to represent the intensity of the lagged effect, and the corresponding lag time was identified as its duration. The analysis is performed as follows:

- (1) Correlate the daily GPP time series with SPEI-5 from the preceding  $m$  days ( $0 \leq m \leq 365$ ), forming a sequence and calculating the correlation coefficient  $R_m$ . Each pixel generates 366 coefficients for different lag times. For example, for a lag time of 60 days, daily SPEI-5 from days 30–243 is correlated with daily GPP from days 90–303 for the 1982–2019 growing season. This process is repeated for lag times from 0 to 365 days. (2) The lag time corresponding to the maximum absolute correlation coefficient  $R_{max\_lag}$  is identified as the time scale of the time-lagged effects, and  $R_{max\_lag}$  represents its intensity.

$$R_m = \text{corr}(GPP, mSPEI), 0 \leq m \leq 365 \quad (3)$$

$$R_{max\_lag} = \begin{cases} \max(R_m), |\max(R_m)| > |\min(R_m)| \\ \min(R_m), |\max(R_m)| < |\min(R_m)| \end{cases} \quad (4)$$

If  $R_{max\_lag} > 0$ , the effect is classified as a positive time-lagged effect (PLE), indicating that delayed drought impact suppresses vegetation productivity, leading to a decline in GPP. Conversely, if  $R_{max\_lag} < 0$ , it is classified as a negative time-lagged effect (NLE), suggesting that GPP increases following a period of drought lag.

### 2.3.4. Determination of the dominant effects of drought

The cumulative and time-lagged effects are compared based on their absolute intensities. The effect with the higher absolute intensity is identified as the dominant drought effect on vegetation GPP. The corresponding intensity and time scale are defined as the dominant effect's intensity and time scale, respectively (Xu et al., 2023).

$$R_{max\_dominant} = \begin{cases} R_{max\_cum}, |R_{max\_cum}| > |R_{max\_lag}| \\ R_{max\_lag}, |R_{max\_cum}| < |R_{max\_lag}| \end{cases} \quad (5)$$

Drought effects on vegetation vary across land-use types and are further influenced by spatial heterogeneity in regional water availability (Comas et al., 2013; Lozano et al., 2020; Peng et al., 2019). To account for these influences, this study further examined the spatial variations of cumulative, time-lagged, and dominant drought effects across different vegetation types and along wetness gradients in the IRB. For each land use category, we extracted the intensity ( $R_{max\_cum}$ ,  $R_{max\_lag}$ ,  $R_{max\_dominant}$ ) and timescale of these effects to assess differences in drought response mechanisms. To evaluate the influence of water availability, this study used the SPEI-360 value on the last day of each year (1982–2019) as a proxy for annual water balance (annual SPEI). Wetness gradients were then classified based on the mean annual SPEI using equal intervals of 0.1.

## 3. Results

### 3.1. Spatiotemporal characteristics of SPEI and GPP

From 1982 to 2019, the mean SPEI in the IRB ranged from  $-0.70$  to  $0.41$ . Approximately 70 % of the basin was classified as "Mildly Dry," mainly distributed west of the Kapchagay Reservoir in Kazakhstan and in the northwestern part of the Ili Kazakh Autonomous Prefecture. The remaining 30 % was classified as "Normal" (Fig. 2a). During the same period, growing season GPP ranged from  $5.02$  to  $1168.75$  g C/m<sup>2</sup>/year, with an average of  $118.38$  g C/m<sup>2</sup>/year, yielding a total multi-year GPP of approximately  $2.05$  Pg C. The spatial distribution of GPP showed significant heterogeneity, with high values concentrated along mountain areas, particularly in the Ili Kazakh Autonomous Prefecture and the southeastern Almaty Region. Low values were observed in river valleys in southeastern Almaty Region and northwest of the Kapchagay Reservoir (Fig. 2d).

According to the MK test results (Fig. 2b–e), the UF curve of the mean SPEI showed an "increasing-decreasing" pattern. A significant intersection between the UF and UB curves in 2006 indicates a climatic shift. Prior to 2006, the basin experienced a wetting trend, which weakened after 2006 and transitioned into a drying trend starting in 2009. In contrast, growing season GPP displayed a continuous upward trend, with a significant intersection in 1992. Before 1992, GPP increased at an accelerating rate, which stabilized afterward. Given the different mutation points of SPEI and GPP, 1992; 2006 were selected as reference points to analyze drought's cumulative and time-lagged effects on vegetation.

Based on segmented linear fitting results (Fig. 2c–f) and the spatial distribution of Sen's slope (Fig. A.2), the mean SPEI exhibited an overall decline from 1982 to 2019, indicating increasing aridity. Drying trends were observed across 88 % of the basin, with significant drying in 10 %, primarily around Lake Balkhash and the eastern Ili Kazakh Autonomous Prefecture. Wetting trends were observed in 12 % of the basin, mainly in the southern Almaty Region. During 1982–1992 and 2006–2019, the basin experienced overall wetting, covering 92 % and 65 % of the area, respectively. In contrast, from 1992 to 2006 was characterized by widespread drying, affecting 66 % of the basin.

From 1982 to 2019, GPP increased across 97 % of the basin, with significant growth in 74 %, particularly in the river valleys of the Ili Kazakh Autonomous Prefecture and the region north of Kapchagay Reservoir. During 1982–1992 and 2006–2019, GPP growth was more pronounced, with increases covering 93 % and 99 % of the basin, respectively. However, between 1992 and 2006, the rate of GPP increase slowed, with 67 % of the area showing improvement.

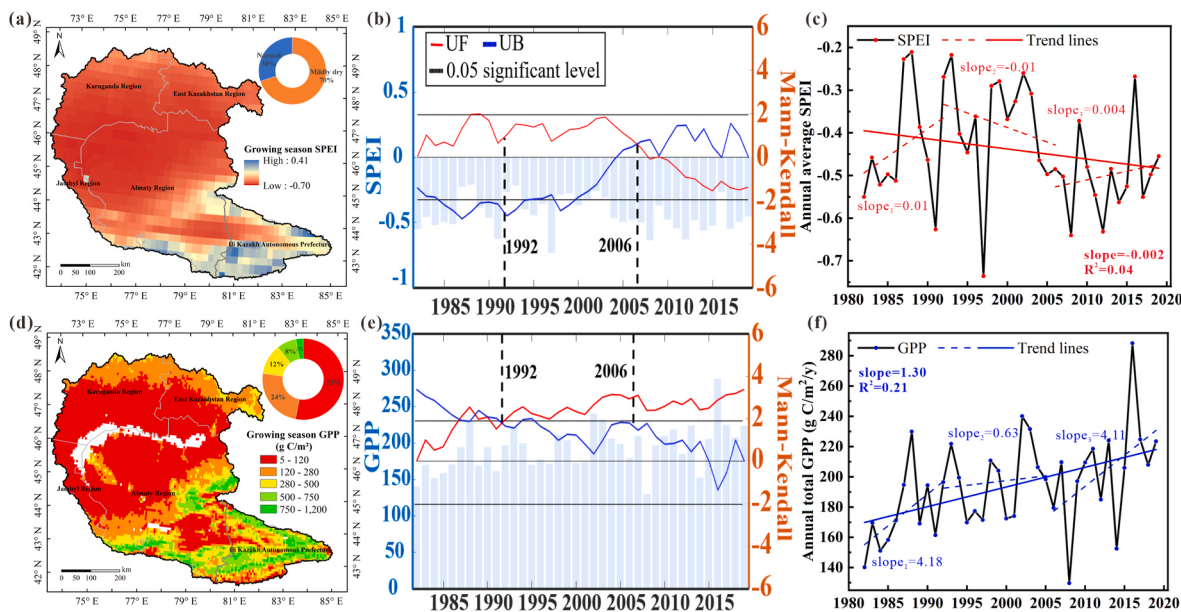


**Fig. 2.** Spatiotemporal dynamics of SPEI and GPP. (a–c) SPEI: spatial distribution, abrupt, and time series; (d–f) GPP: spatial distribution, abrupt, and time series. The variable *slope* indicates the overall trend during the full period (1982–2019); *slope*<sub>1</sub> represents the trend during 1982–1992, *slope*<sub>2</sub> during 1992–2006, and *slope*<sub>3</sub> during 2006–2019.

### 3.2. Cumulative effects of drought on vegetation

As shown in Fig. 3, the correlation between SPEI and GPP varied across different time scales. At the 5-day scale, weak negative correlations were predominant, followed by weak positive correlations. From the 30-day to the 180-day scale, the intensity of positive correlations gradually increased, with over 50 % of the basin exhibiting moderate positive correlations at the 180-day scale. At the 360-day scale, the correlation weakened again, with weak positive correlations dominating most of the region.

The spatial distribution of cumulative effects is illustrated in Fig. 4a–h. From 1982 to 2019, cumulative effect intensity ranged from –0.62 to 0.82, with an average value of 0.47. Approximately 79 % of the basin exhibited a cumulative duration of 180 days. PCE were observed in 94 % of the basin, with particularly high intensities (exceeding 0.8) concentrated in the southwestern part of Almaty Region. In contrast, areas exhibiting NCE accounted for only 6 % of the basin, mainly located along the southern shore of Lake Balkhash, the southeastern Almaty Region, and the northwestern Ili Kazakh Autonomous Prefecture. Across all time periods (Fig. A.3), more than 90 % of the basin consistently exhibited PCE. From 2006 to 2019, the area affected by PCE slightly decreased from 95 % (in the earlier periods) to 93 %, with transitions from PCE to NCE occurring primarily in the river valleys of northern Ili Prefecture. Despite the dominant cumulative duration remaining at 180 days across all three periods, the intensity of PCE has shown a continuous increase since 1982, with particularly notable enhancement in the southwestern Almaty Region.

Fig. 5a, b compares the cumulative drought effects across different vegetation types. Throughout all periods, PCE dominated in grassland, cropland, and bare land. Grassland consistently exhibited the highest proportion of PCE-affected areas, exceeding 96 % in all periods. In contrast, cropland and bare land had relatively lower PCE coverage, with bare land showing a higher proportion of NCE than grassland and cropland. In terms of cumulative days and intensity, grassland exhibited the longest average PCE duration (167 days) and the highest intensity (0.53), with both metrics showing a steady increase since 1982. Cropland experienced a moderate PCE intensity (0.42), but had the shortest cumulative duration among the three land cover types (125 days). Its PCE duration and intensity showed a pattern of initial decline followed

by a later increase, with relatively minor overall variation. Bare land exhibited the lowest PCE intensity (0.29) and a slightly longer duration (131 days) compared to cropland, both of which increased over time. Overall, grassland demonstrated the highest sensitivity to cumulative drought effects, characterized by the most extensive spatial coverage of PCE and the strongest and longest cumulative responses of GPP to prolonged drought stress.

The relationship between mean annual SPEI and cumulative effects is illustrated in Fig. 5c, d. A significant negative correlation was observed between PCE and wetness gradients, in terms of both intensity and duration, whereas NCE exhibited a positive correlation. Specifically, as mean annual SPEI increased (indicating reduced drought severity), both the intensity and duration of PCE declined significantly. The intensity of NCE also decreased notably, while its duration increased slightly. These results suggest that under more severe drought conditions, the suppressive impact of PCE on vegetation productivity becomes stronger and more prolonged. Even in areas exhibiting NCE, vegetation is subjected to stronger effects under drier conditions.

### 3.3. Time-lagged effects of drought on vegetation

Fig. 6 illustrates the correlations between SPEI-5 and GPP across different lag times. As the drought lag time increased from 0 to 365 days, the correlation between SPEI and GPP exhibited a distinct “increase–decrease–increase” pattern. A weak negative correlation was observed at short lag times (0–15 days). Between 15 and 210 days, SPEI and GPP showed a positive correlation, with the strongest positive association occurring at a lag of approximately 120 days. When the lag extended from 210 to 365 days, the correlation turned negative again, reaching its maximum negative intensity around 300 days.

The intensity and duration of time-lagged effects are shown in Fig. 4i–p. From 1982 to 2019, the intensity of time-lagged effects ranged from –0.73 to 0.69, with an average of –0.08. PLE were observed in 42 % of the IRB, primarily distributed across the northern Karaganda Region, East Kazakhstan Region, southeastern Almaty Region, and the northwestern part of the Ili Kazakh Autonomous Prefecture. The mean lag duration in PLE areas was approximately 117 days. In contrast, NLE dominated 58 % of the basin, concentrated mainly in western Almaty Region, the Jambyl Region, and southern Karaganda Region, with an

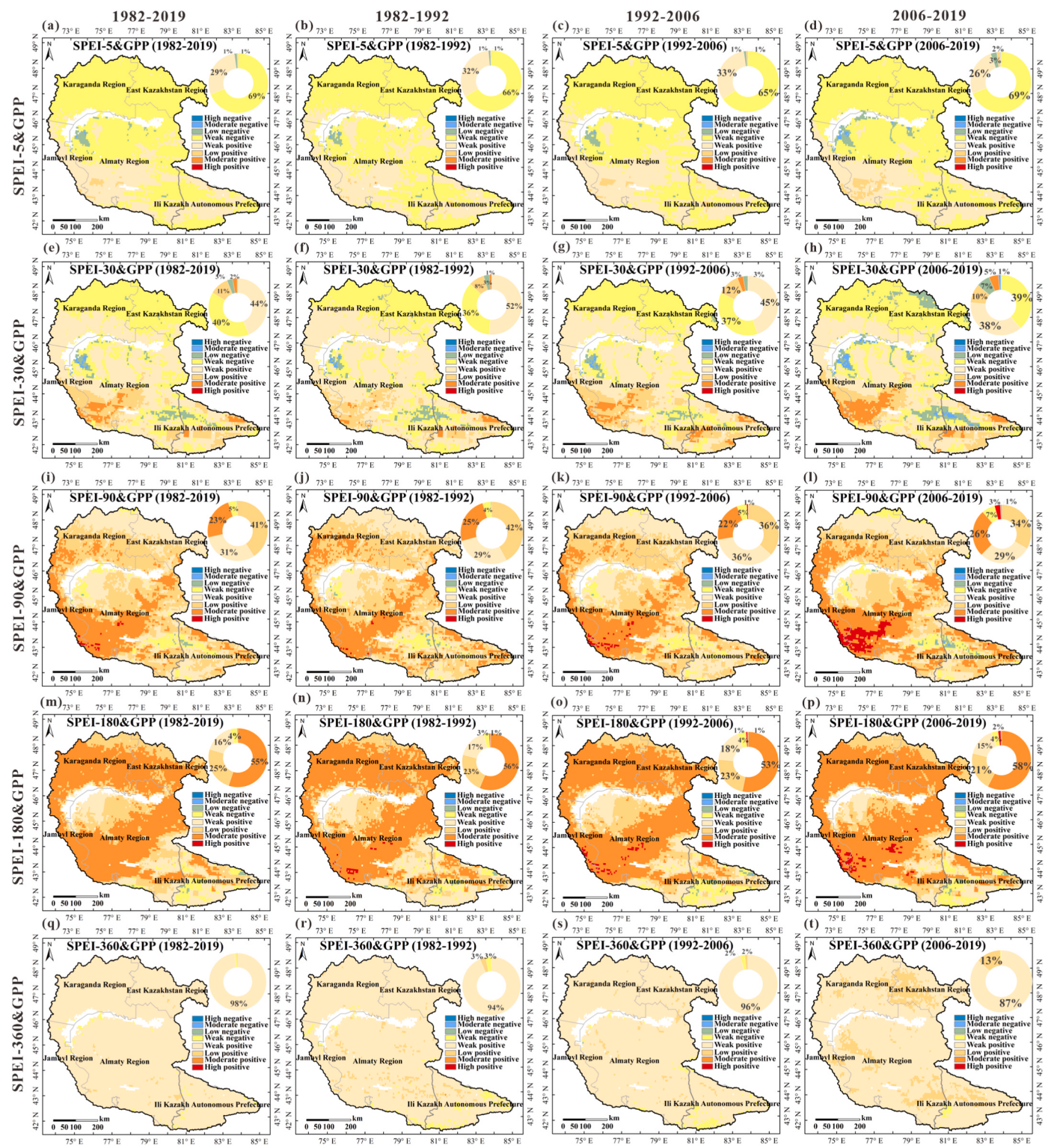


**Fig. 3.** Correlation between SPEI at different time scales and GPP. (a)–(d), (e)–(h), (i)–(l), (m)–(p), and (q)–(t) depict the correlations for SPEI-5, SPEI-30, SPEI-90, SPEI-180, and SPEI-360 with GPP, respectively. The color gradient from red to blue indicates the transition from high positive to high negative correlations.

average lag duration of 280 days. In contrast to cumulative effects that are largely characterized by positive correlations, time-lagged effects show a substantial presence of both positive and negative correlation zones across the basin. During 1982–1992, NLE was dominant, covering over 76 % of the basin with the longest average NLE duration (292 days) and the lowest average intensity (−0.29). PLE covered the remaining 24 % of the area, mainly distributed along the northern and southern shores

of Lake Balkhash, the southeastern Almaty Region, and the southwestern Ili Prefecture. The average lag time for PLE in this period was 118 days. In contrast, the period 1992–2006 saw a significant expansion of PLE, covering 57 % of the basin, and accompanied by a shift to a positive average intensity (0.07). The areas where time-lagged effects transitioned from NLE to PLE were primarily located in the Karaganda Region, East Kazakhstan Region, and the northern part of the Ili Kazakh

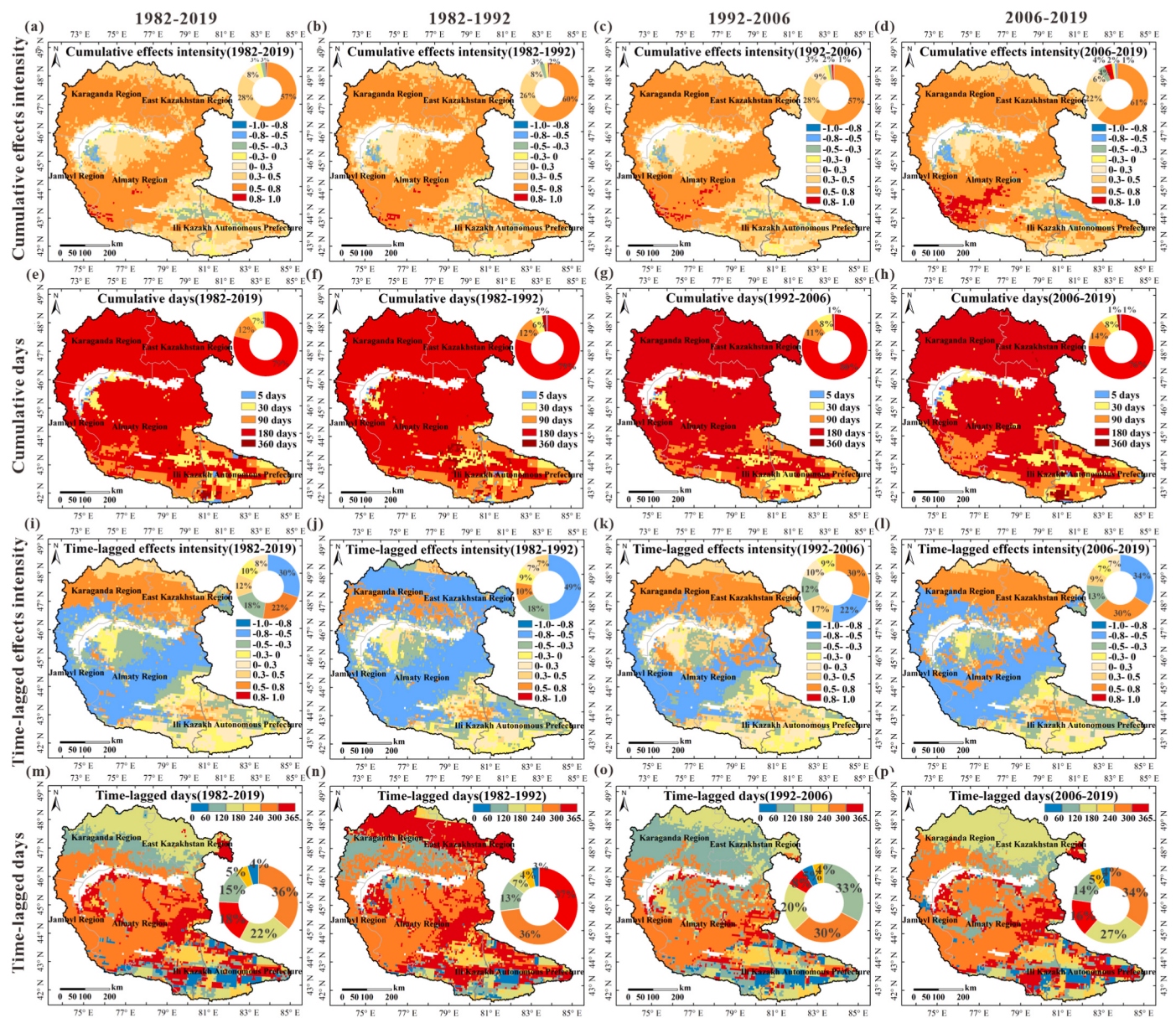


**Fig. 4.** Cumulative and time-lagged effects of drought on GPP. (a-d) Cumulative effects intensity, (e-h) Cumulative days, (i-l) Time-lagged effects intensity, (m-p) Time-lagged days.

Autonomous Prefecture. From 2006 to 2019, the basin experienced a slight re-expansion of NLE, affecting 54 % of the area, while PLE remained substantial at 46 % and exhibited the longest average lag duration (120 days). These findings suggest that in the IRB, vegetation GPP typically declines around 120 days after drought onset and tends to recover or increase approximately 280–300 days later. When the direction of the time-lagged effect is defined based on the relative intensity of these two responses (decline and recovery), it becomes evident that NLE dominated in terms of spatial extent during 1982–1992 and 2006–2019, whereas PLE prevailed during 1992–2006. Although the average lag durations remained relatively stable across the three periods, the intensity of PLE demonstrated a continuous increasing trend over time (Fig. A.4).

Fig. 7a, b illustrates the spatial extent, duration, and intensity of time-lagged drought effects across different land use types. During the period 1982–2019, the proportions of NLE and PLE in grassland were relatively balanced. However, in 1982–1992, NLE dominated, affecting over 70 % of grassland areas. After 1992, the influence of PLE increased markedly, reaching 57 % coverage. Cropland exhibited a similar

pattern: NLE was predominant before 1992, while PLE expanded significantly in the subsequent periods. In contrast, bare land consistently exhibited NLE dominance throughout the entire study period. In terms of lag duration and intensity, PLE durations in grassland and cropland were shorter than those in bare land, whereas NLE durations in grassland and cropland were longer. The intensity of time-lagged effects followed the order: grassland > cropland > bare land. While the intensity of NLE remained relatively stable over time across all land use types, the intensity of PLE showed a clear increasing trend. Overall, grassland exhibited the most pronounced PLE response to drought, with both the affected area and response intensity increasing over time. Cropland showed a milder but similarly upward trend in PLE. In contrast, bare land exhibited the weakest time-lagged response to drought.

Fig. 7c, d illustrates the relationships between mean annual SPEI and the intensity and duration of time-lagged effects. The intensity of PLE exhibited a significant negative correlation with wetness gradients, while the intensity of NLE showed a significant positive correlation. In contrast, the associations between time-lag duration and SPEI were

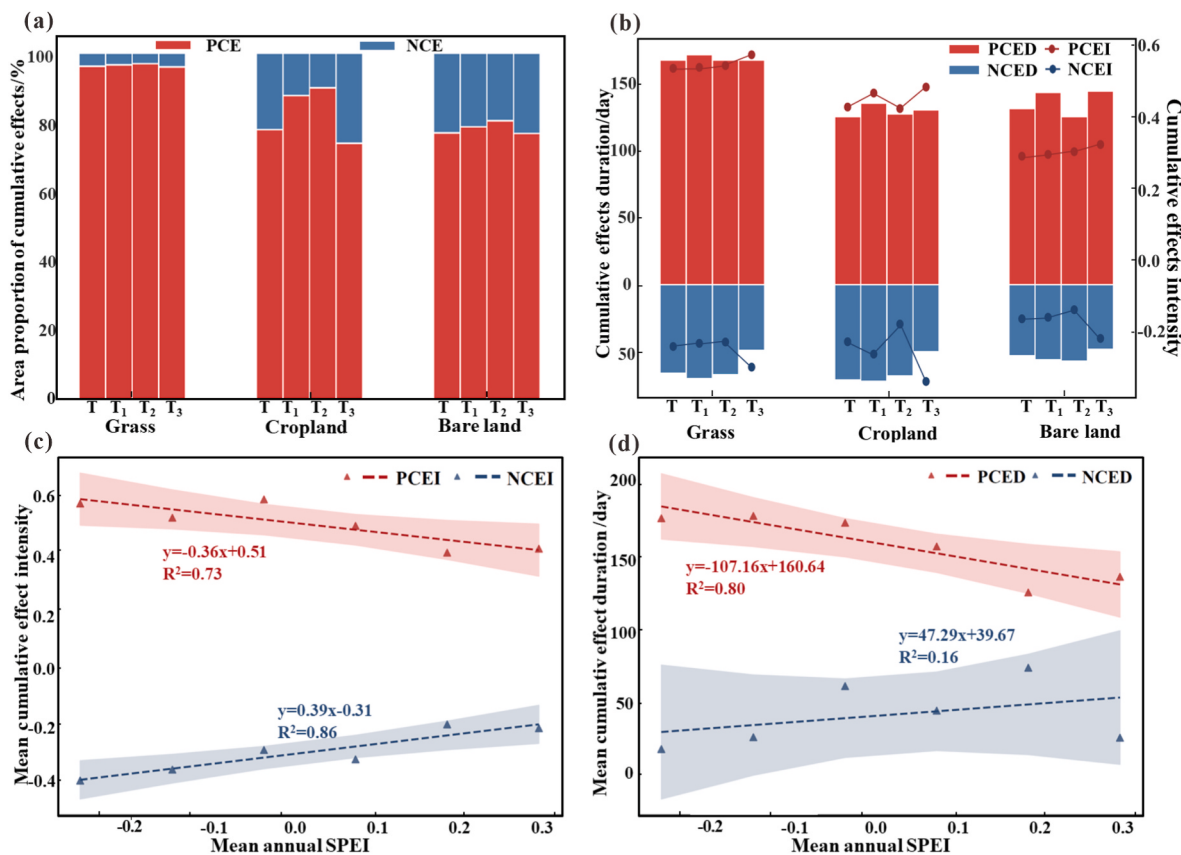


**Fig. 5.** Cumulative effects across vegetation types and along wetness gradients. (a) Area proportion of PCE and NCE by vegetation type and period; (b) Duration and intensity of PCE/NCE; (c) Relationship between PCEI/NCEI and mean annual SPEI; (d) relationship between PCED/NCED and mean annual SPEI. PCEI and NCEI indicate the intensity, while PCED and NCED represent duration. T, T<sub>1</sub>, T<sub>2</sub>, and T<sub>3</sub> refer to the full period (1982–2019), 1982–1992, 1992–2006, and 2006–2019, respectively. Shaded areas indicate the 95 % confidence intervals.

relatively weak. Overall, mean annual SPEI had a stronger influence on the intensity of time-lagged effects than on their duration, indicating that the time-lagged impact of drought on vegetation GPP in the IRB tends to intensify as drought severity increases.

#### 3.4. Dominant influence of cumulative and time-lagged effects of drought on vegetation

The comparison of cumulative and time-lagged effects reveals the dominant drought effects type, intensity, and duration on GPP (Fig. 8). From 1982 to 2019, PCE were the dominant type in 77 % of the basin, with an average duration of 162 days. PLE and NLE accounted for 12 % and 10 % of the area, with average durations of 146 days and 308 days, respectively. Regions dominated by PLE were primarily located in southeastern Almaty Region, northwestern Ili Kazakh Autonomous Prefecture, northern Karaganda Region, and northern East Kazakhstan Region. In contrast, NLE dominated areas were concentrated along the southern shore of Lake Balkhash in Almaty Region. Across the three time periods, PCE consistently dominated over 70 % of the basin, peaking at 80 % during 1992–2006. The spatial extent of PCE-dominated areas exhibited an increasing trend over time. PLE-dominated regions expanded significantly from 6 % in 1982–1992 to 17 % in 2006–2019. In contrast, NLE-dominated areas shrank from 23 % to 9 % over the same periods. Notably, northern Karaganda Region and northern East Kazakhstan Region transitioned from NLE-dominated to PLE-dominated, while areas along the southern shore of Lake Balkhash gradually shifted from NLE to PCE dominance. Additionally, the duration of PLE dominance showed a decreasing trend over time, whereas the durations for PCE and NLE remained relatively stable. The intensities of both PCE and PLE also increased over time when they acted as the

dominant effect type (Fig. A.5).

The dominant effects for different land use types are shown in Fig. 9a, b. Across the entire study period, all three land use types were predominantly affected by PCE, with grassland showing the highest proportion, exceeding 70 %. In comparison, PLE and NLE accounted for smaller proportions and exhibited distinct temporal trends. NCE dominated areas were primarily found in cropland and bare land, accounting for less than 1 % of the entire basin. The proportion of PLE increased over time in both grassland and cropland, exceeding 15 % during 2006–2019. In contrast, the proportion of NLE declined across all land types, particularly in grassland, where it decreased from approximately 21 % in 1982–1992 to 7 % in 2006–2019. In terms of duration, PCE and PLE lasted between 110 and 200 days on average, whereas NLE generally persisted longer, ranging from approximately 235 to 300 days. Nevertheless, the intensity of both PCE and PLE increased over time, while changes in NLE intensity were relatively minor. Overall, grassland exhibited the strongest PCE response to drought, characterized by the largest PCE dominated area and the highest response intensity.

The relationships between mean SPEI and the dominant effects are shown in Fig. 9c–e. Although the intensity of NCE exhibited a positive correlation with SPEI, NCE-dominated areas accounted for less than 1 % of the basin and were therefore excluded from further analysis. The area proportion, intensity, and response duration of PCE-dominated regions showed significant negative correlations with mean annual SPEI, indicating that as drought severity increases, PCE is more likely to become the dominant effect type, with stronger impacts and longer durations.

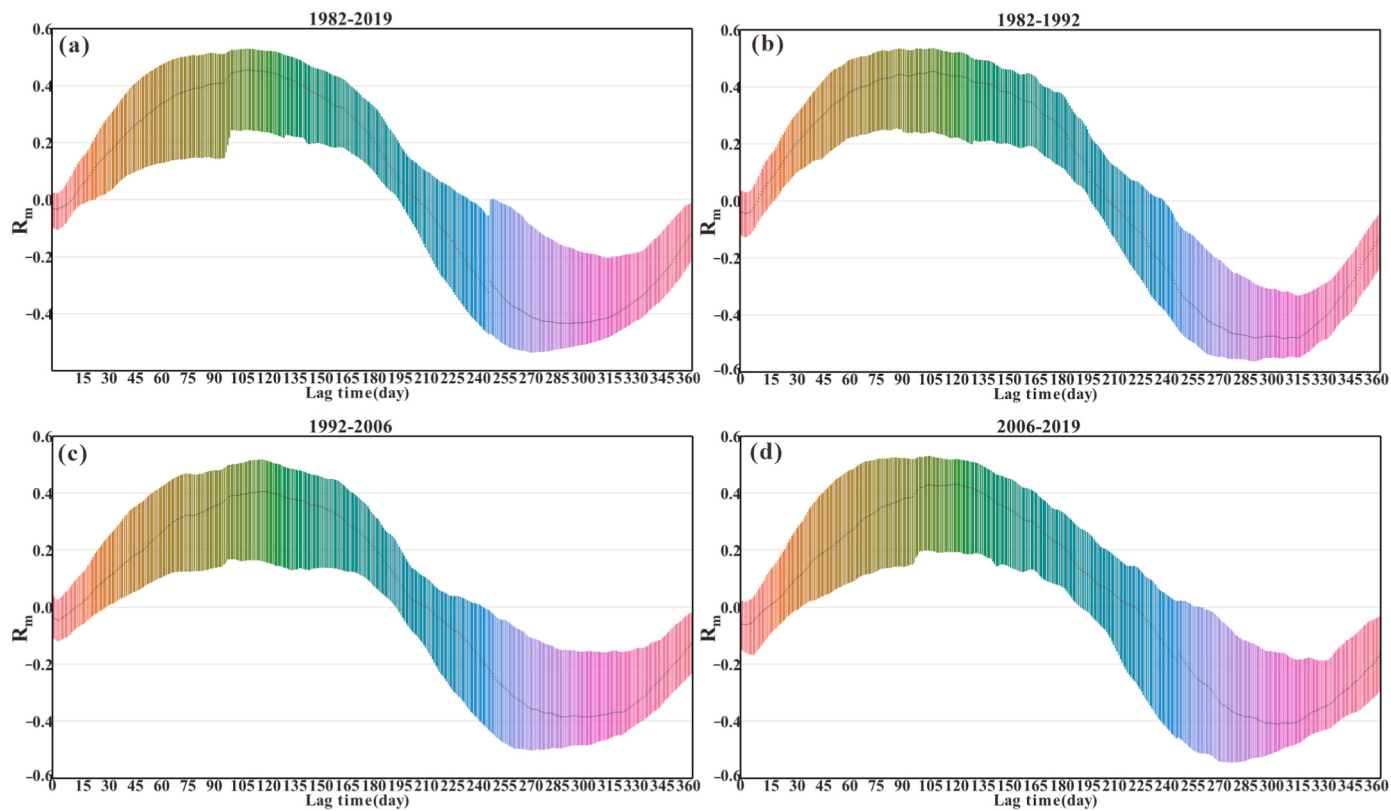


**Fig. 6.** Correlation coefficients between SPEI and GPP at different lag times. (a) 1982–2019, (b) 1982–1992, (c) 1992–2006, and (d) 2006–2019. The black line represents the spatial median correlation across lag times, while the upper and lower ends of the colored bars indicate the upper and lower quartiles, respectively.

#### 4. Discussion

##### 4.1. Cumulative effects on GPP and their seasonal characteristics

This study utilized long-term, high-resolution daily GPP data in combination with multi-scale SPEI to investigate the cumulative, lagged, and dominant effects of drought on vegetation productivity across the IRB. By elevating the temporal resolution from the conventional monthly or seasonal scale to the daily scale, this research provides a more precise characterization of vegetation responses to drought stress in arid regions. The results reveal that in most areas of the IRB, GPP exhibits the strongest positive correlation with cumulative drought conditions over the preceding 180 or 90 days. Negative correlations were observed only in a few regions, including the southern shore of Lake Balkhash, southeastern Almaty Region, and northwestern Ili Kazakh Autonomous Prefecture. These findings are consistent with those of Liu et al. (2023a, 2023b), who reported similar drought cumulative durations in Central Asia. As a core region of the Central Asian arid zone, the IRB demonstrates a typical vegetation response to prolonged water stress. After the onset of drought, the continued depletion of soil moisture does not immediately suppress vegetation growth. However, repeated drought events gradually accumulate physiological stress. Over time, this stress can exceed the ecological threshold of vegetation tolerance, resulting in a significant decline in GPP. This process highlights the cumulative nature of drought impacts. While short-term droughts may have limited effects on vegetation productivity, prolonged or recurrent drought events can exert substantial inhibitory effects on carbon fixation, ultimately affecting overall ecosystem productivity and carbon cycling processes (van der Molen et al., 2011). Interestingly, the regions exhibiting negative cumulative effects contradict the conventional expectation that drought necessarily suppresses vegetation growth. This phenomenon can be attributed to the strong physiological adaptability of vegetation in arid environments.

Such vegetation can develop deeper root systems and finer root hairs to access water from deeper soil layers, modify leaf morphology (e.g., increased leaf thickness or reduced leaf area), and regulate stomatal behavior to minimize transpiration. These adaptive traits enable vegetation to maintain relatively high GPP even under limited water availability (Liu et al., 2023b; Zhang et al., 2018b).

Different vegetation types exhibit distinct cumulative responses to drought. Forests tend to be less sensitive to drought due to their deeper root systems and greater water storage capacity. In contrast, grasslands are generally more vulnerable to drought stress because of their shallow root systems, which limit access to deeper soil moisture (Deng et al., 2022). Croplands are often subject to anthropogenic management practices such as irrigation and fertilization, which can mitigate the impacts of drought to some extent. However, rainfed croplands are typically more susceptible to drought than irrigated croplands (He et al., 2020; Azadi et al., 2018). Bare land, characterized by low vegetation cover and limited soil water-holding capacity, has minimal water demand and thus is the least affected by drought (Blazin and Sterk, 2013). As a result, compared to croplands and bare land, grasslands in the IRB exhibit the strongest cumulative response to drought (Fig. 5a, b).

The intensity and duration of drought cumulative effects show a significant linear relationship with the wetness gradient (Fig. 5c, d). Specifically, as the annual mean SPEI increases (indicating reduced drought severity), both the intensity and duration of PCE decrease significantly. Similar linear patterns have been reported in previous studies (Peng et al., 2019; Zhao et al., 2020), whereas other research has observed nonlinear drought responses along moisture gradients (Konings et al., 2021; Xu et al., 2021). Such discrepancies may be attributed to differences in regional drought intensity, vegetation type, and other ecosystem characteristics. In the IRB, located in the core of Central Asia's arid zone, soil moisture is the primary driver of vegetation growth (Yu et al., 2025; Xu et al., 2023). In regions with lower annual mean SPEI, low precipitation and high evapotranspiration result in

long-term soil moisture deficits. These conditions facilitate the accumulation of drought impacts, resulting in prolonged GPP decline and delayed recovery, which leads to stronger and longer-lasting PCE (Peng et al., 2019). In contrast, regions with higher annual SPEI receive more rainfall, helping to reduce moisture deficits and promote faster recovery, thereby weakening the cumulative effects. Moreover, this study uses long-term mean SPEI as an indicator of wetness gradient, which captures the steady-state climatic water availability. This helps explain the observed linear relationship, as it reflects long-term vegetation responses rather than short-term variability. Given the progressive aridification trend in the IRB since 1982, the intensity of drought cumulative effects has also increased accordingly.

To investigate the seasonal differences in drought cumulative effects on vegetation GPP in the IRB, the growing season was divided into spring (April–May, days 90–151), summer (June–August, days 152–243), and autumn (September–October, days 244–303). As shown in Fig. 10a, b, NCE dominates in spring, with relatively strong intensity. This may reflect short-term physiological adaptation or resource reallocation triggered by spring drought, resulting in a delayed or even slightly enhanced GPP response. In summer, PCE becomes dominant across all land cover types, with proportions exceeding 90 %, and reaching up to 99 % in grasslands. PCE intensity is also significantly higher in summer than in spring or autumn, indicating that drought in summer imposes stronger and more persistent suppression on GPP. In autumn, PCE still dominates, but with reduced spatial extent and intensity compared to summer. These seasonal differences are closely related to vegetation water demand, physiological status, and meteorological conditions. In spring, vegetation is in its early growth phase, characterized by incomplete canopy development and limited root activity (Sullivan and Eastin, 1975). In addition, snowmelt during this period can partially replenish soil moisture (Fang et al., 2019). As a result, moderate drought may not immediately suppress GPP, as vegetation can rely on short-term adaptation mechanisms and residual moisture to sustain growth. In summer, rising temperatures and intensified evapotranspiration increase vegetation water dependence (Knapp and Smith, 2001). Drought during this period leads to more pronounced GPP reduction, especially in grasslands, which are more sensitive to hot and dry conditions. In autumn, as temperatures decline and photosynthetic activity slows, vegetation enters a senescence phase (Huang et al., 2024). Although drought still affects GPP, its impact is less severe than in summer. To mitigate the cumulative impacts of drought on vegetation productivity in the IRB, targeted ecological management strategies should be implemented according to both season and land use type. In spring, priority should be given to soil moisture monitoring, drought early warning systems, and the optimization of sowing and irrigation schedules to avoid early-stage stress. Summer represents the critical period for drought regulation, especially in grassland areas, where practices such as rotational grazing, supplementary irrigation, and grazing exclusion can improve soil water retention and enhance ecosystem drought resilience. In autumn, management should focus on restorative measures and biomass conservation. Implementing fallow periods during this time can help promote energy storage and support vegetation recovery in the subsequent growing season.

#### 4.2. Time-lagged effects on GPP and their seasonal characteristics

Unlike most previous studies that analyzed drought lag effects at a monthly scale (0–12 months), yielding only 13 discrete lag intervals, this study improves temporal resolution to a daily scale and systematically evaluates the correlation between SPEI-5 and GPP over a full range of 0–365 days. This high-resolution approach allows for a more continuous and detailed understanding of the lagged response of vegetation to drought. Results show that the correlation coefficients exhibit a distinct "rise–fall–rise" trend as lag days increases, alternating between positive and negative values (Fig. 6). At short lags (0–15 days), SPEI reflects recent water conditions, while GPP is more directly influenced by

immediate factors such as radiation and temperature. In this phase, mild short-term drought may even induce compensatory growth or internal carbon reallocation, resulting in weak or negative correlations. As lag time increases to 15–210 days, earlier drought conditions begin to accumulate through their impact on soil moisture, root growth, and leaf area development, leading to sustained suppression of GPP. This results in stronger positive correlations, peaking at around a 120-day lag, when GPP most clearly reflects the delayed effects of prior drought stress. When the lag extends beyond 210 days, SPEI reflects water conditions during the previous autumn, winter, or even the previous growing season. Following drought stress, some vegetation may exhibit compensatory growth in the subsequent year through mechanisms such as resource reallocation, utilization of stored carbon reserves, and rapid regrowth. At a 300-day lag, SPEI reflects moisture conditions from the previous summer to early autumn, the peak growing season of the prior year. Abundant rainfall and vigorous growth during that time can raise evapotranspiration, intensify competition, and dilute nutrients in the following season, ultimately reducing current-year GPP. Conversely, if the previous year was severely dry, limited biomass accumulation and reduced competition may have preserved soil moisture and facilitated rapid vegetation recovery in the current season. These patterns highlight the complex and delayed responses of ecosystems to drought stress over time.

Unlike the cumulative effects that are dominated by positive correlations, time-lagged effects in the IRB display both positive and negative patterns (Fig. 4i–l). From 1982 to 2019, PLE covered 42 % of the basin with a mean delay of 117 days, whereas NLE occupied 58 % with an average delay of 280 days. Thus, compensatory increases in GPP after drought are both more widespread and stronger than the shorter positive responses. Compared with the shorter lags reported for Xinjiang grasslands (1–3 months, Liu et al., 2023c) and Central Asian grasslands (2–3 months, Lu et al., 2023), the longer lags detected here can be explained by three factors: (1) daily temporal resolution that resolves finer response phases, (2) spatial heterogeneity in drought intensity, vegetation type and management, and (3) the inclusion of negative-correlation pixels by using the maximum absolute correlation rather than only the maximum positive value. Similar NLE have been documented in the northern Central Asian steppe, the Kazakh Plain and the Lake Balkhash region (Xu et al., 2023; Liu et al., 2023b). First, plants adopt physiological adjustments such as deeper rooting, more root hairs, altered leaf morphology, and stricter stomatal control. These traits help maintain or even increase productivity during drought (Chen et al., 2013; Schwinnig and Sala, 2004; Lian et al., 2021). After the stress subsides, stored carbon and reallocated resources fuel a rebound in growth. Second, severe drought and concurrent warming in the previous year can accelerate alpine snowmelt. The resulting meltwater markedly raises early-spring soil moisture (Huang et al., 2024), and a Birch-effect nutrient pulse further stimulates photosynthesis and biomass accumulation (Jarvis et al., 2007). This combination produces negative correlations at lags of about 280–300 days. Third, post-drought human interventions in farming and grazing areas, including supplementary irrigation, reduced grazing, and fallowing, can elevate GPP in the subsequent growing season (Guo et al., 2024).

Compared with croplands and bare lands, grasslands in the IRB show the strongest drought time-lagged effects (Fig. 7a, b). This contrast arises from both ecological traits and management practices. First, grassland species have shallow root systems that depend on surface soil moisture (Deng et al., 2022). Second, most grasslands are natural or semi-natural and receive little irrigation or fertilization, so they rely entirely on rainfall and snowmelt, which enhances drought time-lagged effects. Third, the high proportion of perennial grasses and forbs enables plants to down-regulate growth during drought, conserve carbohydrates, and then mobilize these reserves for vigorous regrowth in the following season (Chaves et al., 2003), amplifying negative or positive lag responses. In contrast, croplands often benefit from irrigation, fertilization, tillage, and crop rotation, which buffer drought impacts and

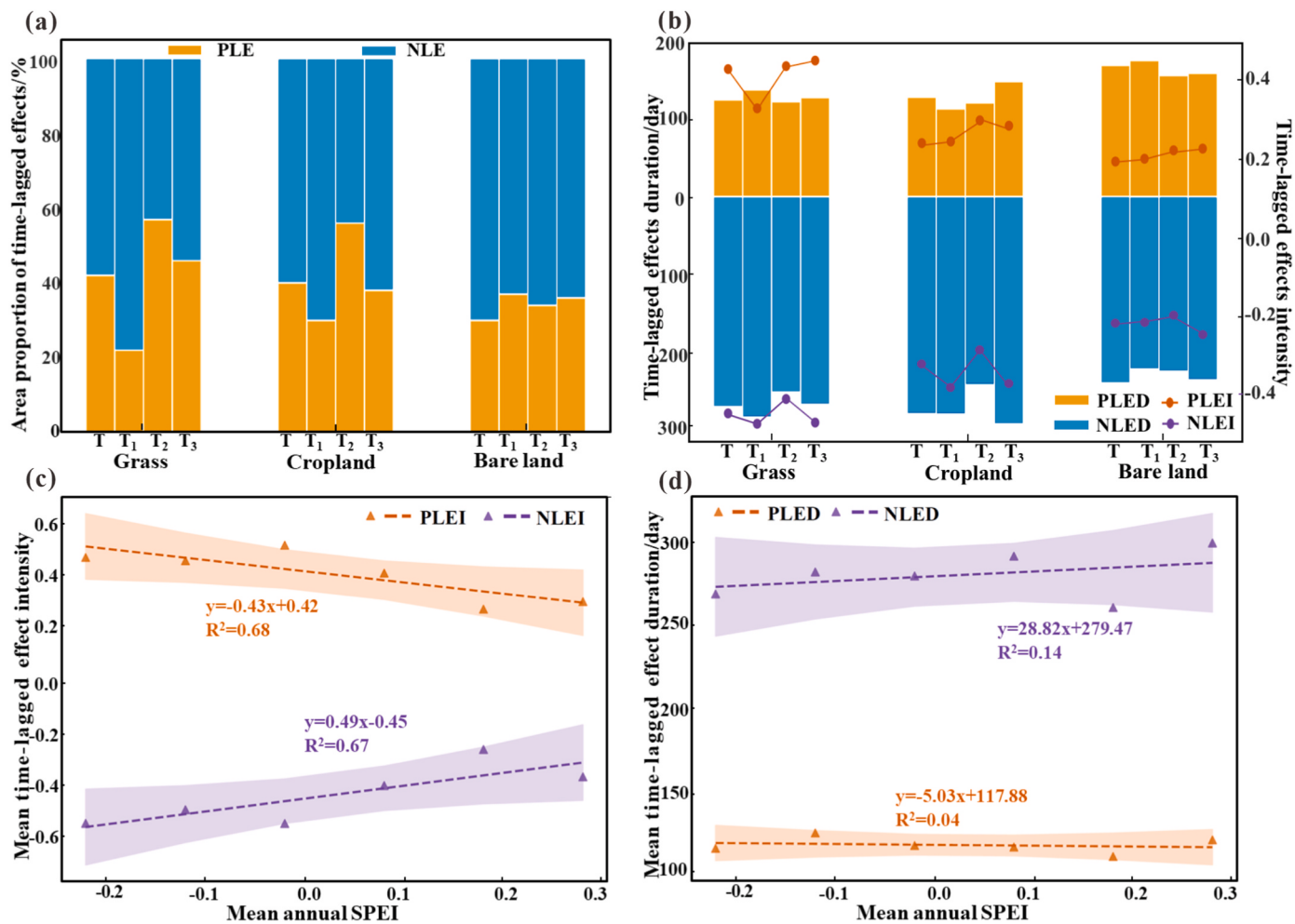


**Fig. 7.** Time-lagged effects across vegetation types and along the wetness gradients. (a) Area proportion of PLE and NLE by vegetation type and period; (b) Duration and intensity of PLE/NLE; (c) Relationship between PLEI/NLEI and mean annual SPEI; (d) Relationship between PLED/NLED and mean annual SPEI. PLEI and NLEI indicate intensity, while PLED and NLED represent duration. T, T<sub>1</sub>, T<sub>2</sub>, and T<sub>3</sub> are defined as in Fig. 5. Shaded areas indicate the 95 % confidence intervals.

shorten lag effects even in rainfed fields (He et al., 2020; Azadi et al., 2018). Bare land has minimal vegetation, low evapotranspiration, and a small productivity baseline, so its lag responses are weakest (Biazin and Sterk, 2013). The relationship between time-lagged effects and the wetness gradient indicates that lagged GPP responses intensify as aridity increases, whereas variations in lag duration are not significant (Fig. 7c, d). Xu et al. (2023) and Liu et al. (2023b) reported similar patterns: in drier areas, repeated or prolonged soil-moisture deficits push vegetation closer to its physiological limits, producing stronger delayed impacts on productivity. In contrast, lag duration appears to be governed more by plant phenology, rooting depth, and the timing of management interventions than by the long-term wetness gradients.

Fig. 10c, d reveals clear seasonal contrasts in time-lagged effects. In spring, PLE dominate all land use types, occupying 80–95 % of basin with lag times of 155–198 days. Grasslands show the greatest PLE intensity and duration, indicating that moisture deficits from the previous year continue to suppress growth. During summer, when vegetation reaches its rapid growth phase, PLE area, intensity, and duration decline, while NLE expand in cropland and bare land, reflecting heightened sensitivity to antecedent drought despite the onset of compensatory growth. In autumn, PLE weakens further in cropland and bare land, and cropland shifts to NLE dominance with lags extending to 327 days; grassland PLE area rebounds slightly but its intensity keeps decreasing. Across the three seasons, grassland shows the strongest lag effects, cropland displays intermediate responses, and bare land the weakest. Positive lag effects last longer on bare land, whereas negative

lag effects persist longer on grassland and cropland. In spring, lagged suppression is strongest but vegetation sensitivity is low. Summer marks a critical shift from suppression to compensation and shows the highest drought sensitivity (Huang et al., 2024). Autumn brings conditions that favor vegetation recovery, particularly in cropland. Management should therefore prioritize springtime water conservation, timely irrigation, and reduced grazing to ease lagged suppression. During summer, managers need close moisture monitoring, precision irrigation, and rotational or short-term grazing bans to avoid further stress. In autumn, fallowing, organic amendments, and enclosure can harness compensatory growth, boosting carbon uptake and productivity.

At the pixel scale, this study compared cumulative effects with time-lagged effects to identify the dominant response. Throughout the study period, PCE dominated all land-use types, and grasslands showed the strongest response with both the largest share of PCE-affected pixels and the highest intensity. Moreover, as regional aridity intensified, PCE became increasingly dominant and exhibited greater magnitude and longer duration (Fig. 9). Earlier work has shown that vegetation growth is closely controlled by the cumulative effects of climatic factors (Wen et al., 2019; Liu et al., 2021a), and Yang et al. (2023) found that such cumulative effects dominate across most of Central Asia. Seasonal analysis shows that PCE dominance is strongest in summer, somewhat weaker in autumn, and in spring is often supplanted by PLE or NLE (Fig. A.6). This pattern likely reflects seasonal shifts in growth rate and water-nutrient demand across phenological stages (Zhang et al., 2018a). In general, drought impacts on vegetation accumulate over long periods,

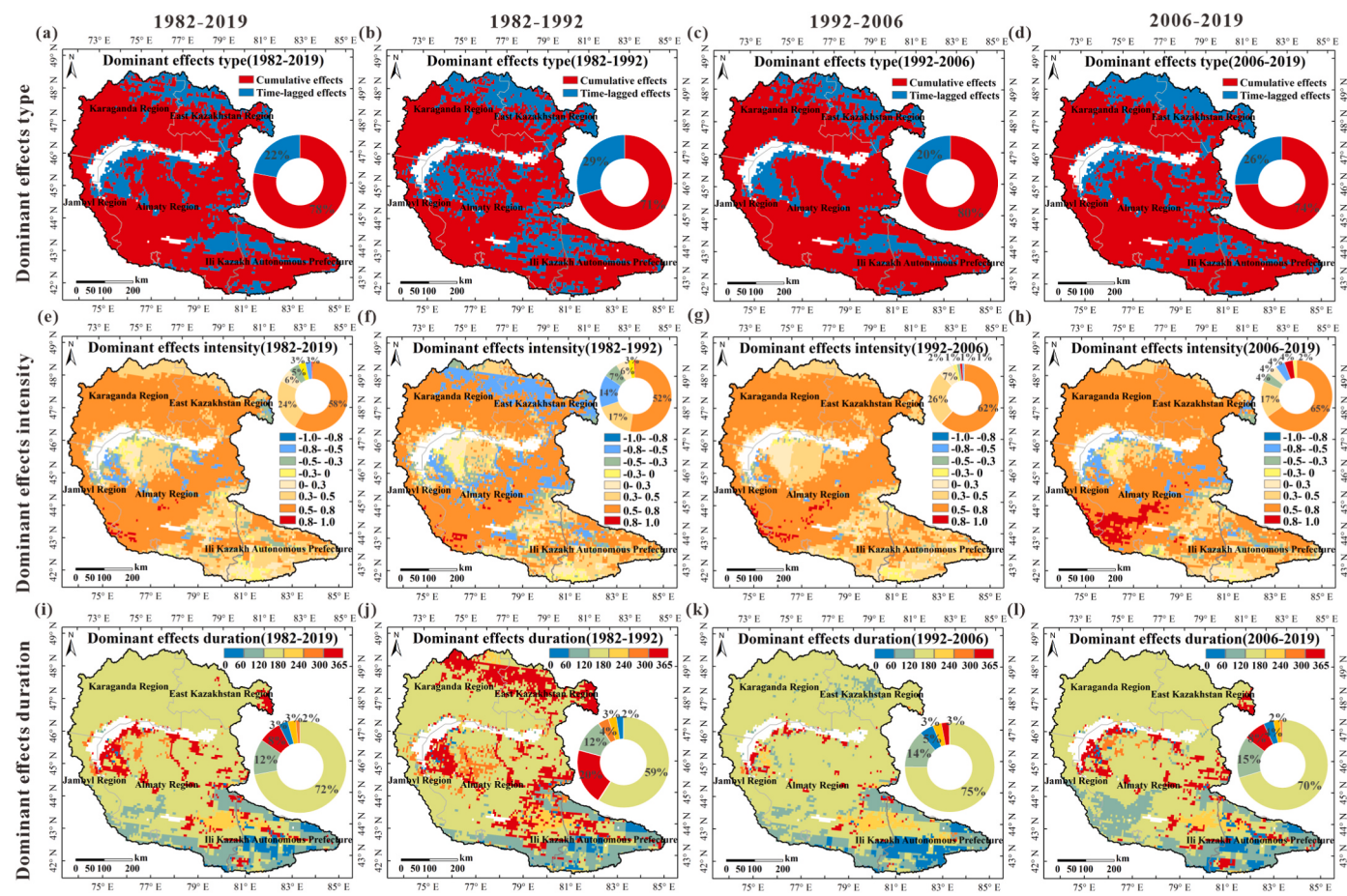


Fig. 8. Spatiotemporal patterns of dominant drought effects on GPP. (a-d) Type; (e-h) Intensity; (i-l) Duration.

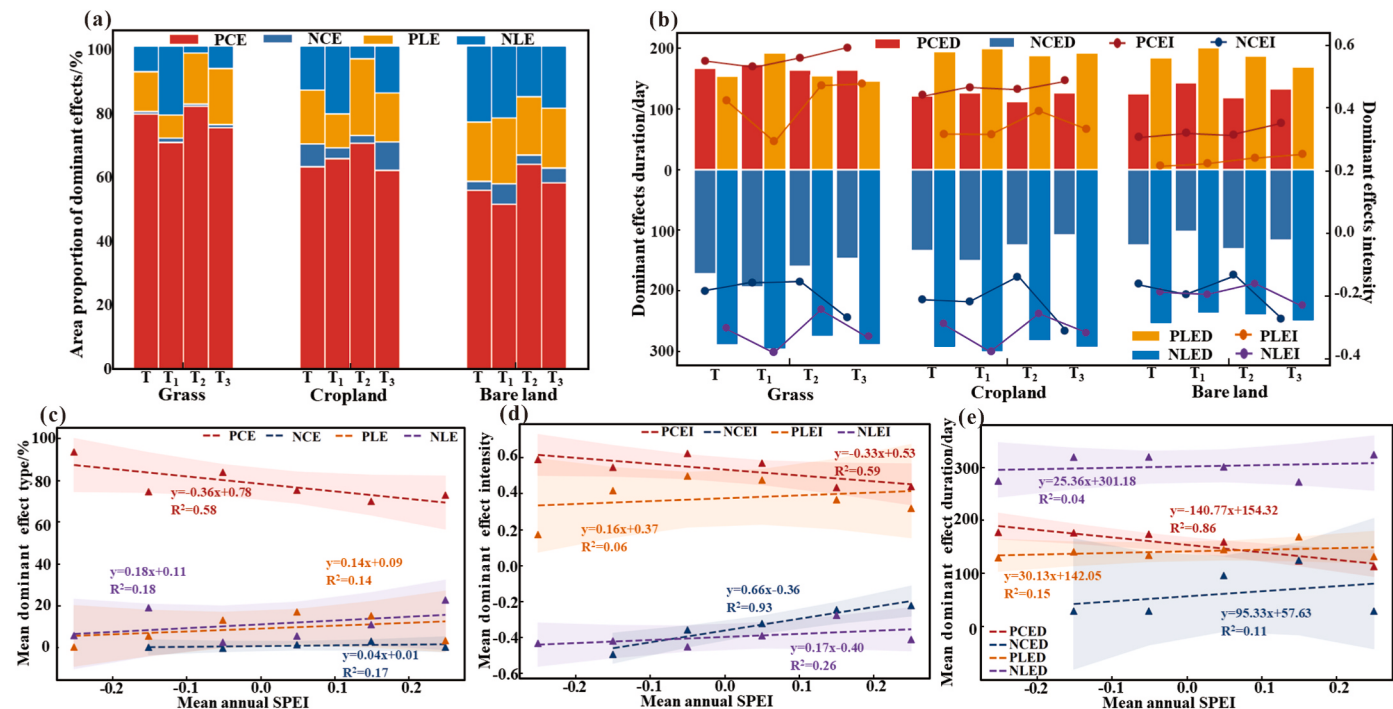
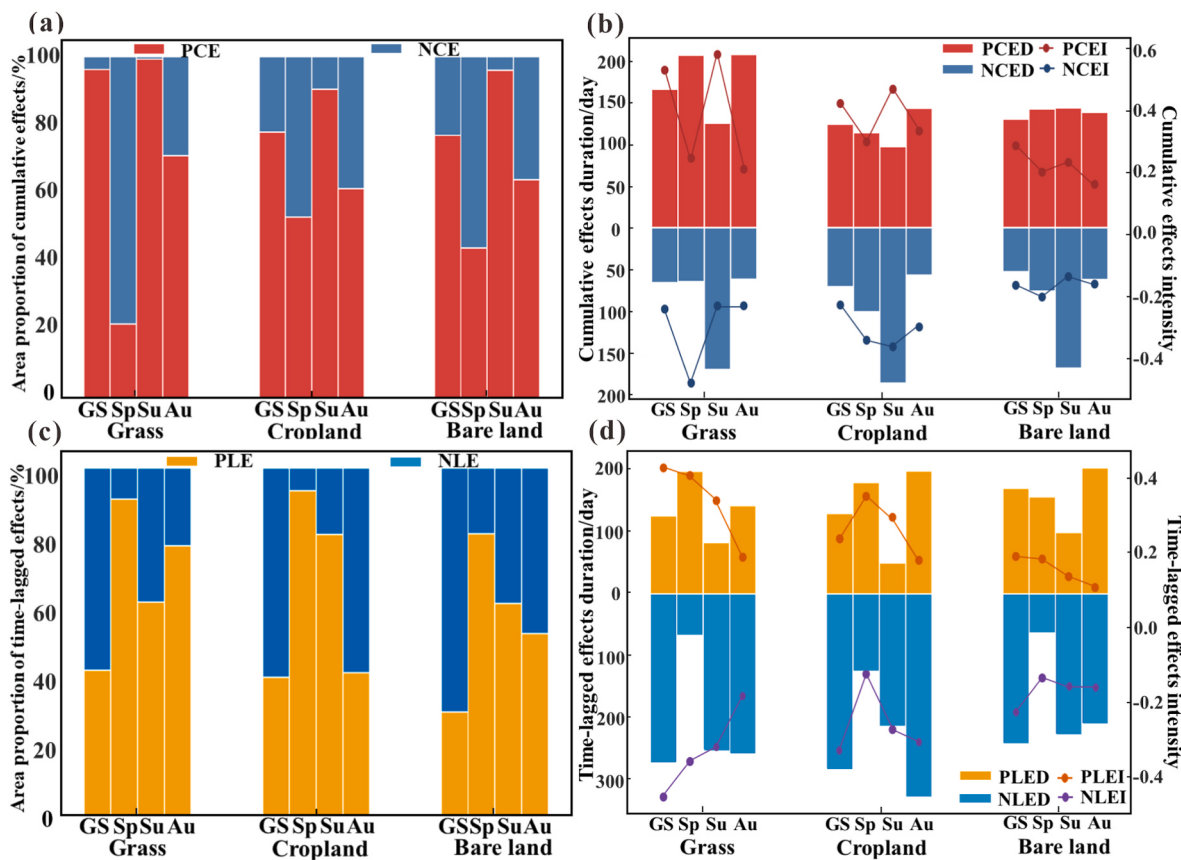


Fig. 9. Dominant effects across vegetation types and along the wetness gradients. (a) Area proportion; (b) Duration and intensity by vegetation type and period; (c-e) Relationships between dominant effect type, intensity, duration and mean annual SPEI. T, T<sub>1</sub>, T<sub>2</sub>, and T<sub>3</sub> are defined as in Fig. 5. Shaded areas indicate the 95 % confidence intervals.



**Fig. 10.** Seasonal differences in drought cumulative and time-lagged effects. (a) Proportion of cumulative effects area under three land use types across different seasons; (b) Intensity and duration of cumulative effects; (c) Proportion of time-lagged effects area; (d) Intensity and duration of lag effects. GS, Sp, Su, and Au represent the growing season, spring, summer, and autumn, respectively.

whereas lag effects capture only a momentary response and overlook ongoing post-drought dynamics (Wu and Wang, 2022). Future studies should therefore place greater emphasis on cumulative drought effects to better elucidate the complex interplay between climate change and vegetation dynamics.

#### 4.3. Uncertainties and future directions

This study investigated the response and cumulative and time-lagged effects of drought on vegetation GPP in the IRB, advancing the analysis resolution from the commonly used monthly scale to a finer daily scale. However, certain uncertainties remain. First, the mechanisms by which climate change affects vegetation are complex and regionally variable. This study focused solely on the impact of meteorological drought, without considering other natural factors (e.g., vapor pressure deficit, soil moisture, temperature, solar radiation) or human activities (e.g., grazing, irrigation, fertilization) that also influence vegetation growth. Future research should quantify the relationships between vegetation dynamics and drought characteristics, additional environmental variables, and human activity intensity to improve the accuracy of drought impact and ecosystem response assessments. Second, this study considered only single meteorological drought events, without addressing the potential effects of compound or persistent droughts. Finally, although the temporal resolution was improved to a daily scale, the low spatial resolution of global SPEI datasets introduced uncertainties during spatial interpolation. Future work should consider using higher-resolution drought indices or developing fusion models to integrate fine-scale data with drought indicators, enabling a more comprehensive and accurate understanding of vegetation-climate interactions.

#### 5. Conclusions

This study refines the assessment of drought–vegetation interactions from the traditional monthly scale to a high-resolution daily scale, focusing on the ecologically representative Ili River Basin in Central Asia. By integrating daily GPP and multi-scale SPEI data, it constructs a continuous 0–365 days lag window to comprehensively evaluate cumulative, time-lagged, and dominant drought effects in terms of intensity, duration, and direction. These effects are further analyzed across land use types, wetness gradients, and seasons, and fine-scale ecosystem management strategies are proposed.

Key findings include: (1) Over the past four decades, growing season GPP showed a significant increasing trend ( $k = 1.302 \text{ g C/m}^2/\text{a}$ ), while SPEI indicated a shift toward drier conditions ( $k = -0.002/\text{a}$ ), with abrupt changes in 1992 and 2006. (2) Cumulative drought effects suppressed GPP in over 90 % of the basin, with accumulation durations clustered around 180 and 90 days. Stronger droughts led to more intense and prolonged cumulative impacts. (3) The correlation between SPEI and GPP followed a rise–fall–rise pattern with increasing lag time, shifting from positive to negative. Time-lagged effects were spatially complex, with 58 % of the basin showing peak GPP recovery after 280 days, and 42 percent exhibiting strongest suppression after 117 days. Lag intensity increased with drought severity. (4) Cumulative effects were dominant in 77 % of the basin and became more prevalent with increasing drought severity. (5) Spring showed strong lagged suppression but low sensitivity; summer exhibited the most intense and sensitive cumulative suppression; and autumn showed signs of compensatory recovery. Among land use types, grassland exhibited the highest sensitivity to drought.

These findings highlight the need for differentiated drought

management strategies tailored to seasonal and land use conditions, with emphasis on enhancing drought monitoring and water regulation in spring and summer. Grassland ecosystems should be prioritized in future drought risk mitigation and adaptive planning. Overall, this study enhances the understanding of ecosystem carbon dynamics under climate change and provides scientific support for drought mitigation and adaptation in agricultural and pastoral systems.

### CRediT authorship contribution statement

**Mengzhen Huang:** Writing – original draft, Visualization, Methodology, Data curation. **Ruijie Lu:** Writing – review & editing, Project administration. **Zhiyong Zhang:** Investigation. **Yue Zhou:** Validation, Investigation. **Peiru Li:** Investigation, Formal analysis. **Peng Du:** Investigation. **Tian Zhao:** Investigation. **Sining Xiao:** Investigation.

### Declaration of competing interest

The authors declare that they have no known competing financial interests or personal relationships that could have appeared to influence the work reported in this paper.

### Acknowledgments

This research was funded by the Third Xinjiang Scientific Expedition Program, grant number 2022xjkk0600. The authors thank the editor and anonymous reviewers for their valuable comments and suggestions on an earlier version of the paper, which resulted in a more complete and accelerated presentation of the work performed.

### Appendix A. Supplementary data

Supplementary data to this article can be found online at <https://doi.org/10.1016/j.jenvman.2025.126670>.

### Data availability

Data will be made available on request.

### References

- Anav, A., Friedlingstein, P., Beer, C., Ciais, P., Harper, A., Jones, C., Zhao, M., 2015. Spatiotemporal patterns of terrestrial gross primary production: a review. *Rev. Geophys.* 53 (3), 785–818. <https://doi.org/10.1002/2015RG000483>.
- Arora, V.K., 2002. The use of the aridity index to assess climate change effect on annual runoff. *J. Hydrol.* 265 (1–4), 164–177. [https://doi.org/10.1016/S0022-1694\(02\)00101-4](https://doi.org/10.1016/S0022-1694(02)00101-4).
- Azadi, H., Keramati, P., Taheri, F., Rafiaani, P., Teklemariam, D., Gebrehiwot, K., Witlox, F., 2018. Agricultural land conversion: reviewing drought impacts and coping strategies. *Int. J. Disaster Risk Reduct.* 31, 184–195. <https://doi.org/10.1016/j.ijdr.2018.05.003>.
- Biazin, B., Sterk, G., 2013. Drought vulnerability drives land-use and land cover changes in the rift valley dry lands of Ethiopia. *Agric. Ecosyst. Environ.* 164, 100–113. <https://doi.org/10.1016/j.agee.2012.09.012>.
- Braswell, B.H., Schimel, D.S., Linder, E., Moore, B.H., 1997. The response of global terrestrial ecosystems to interannual temperature variability. *Science* 278 (5339), 870–873. <https://doi.org/10.1126/science.278.5339.870>.
- Chaves, M.M., Maroco, J.P., Pereira, J.S., 2003. Understanding plant responses to drought—from genes to the whole plant. *Funct. Plant Biol.* 30 (3), 239–264. <https://doi.org/10.1071/FP02076>.
- Chen, Y., Zhou, H., Chen, Y., 2013. Adaptation strategies of desert riparian forest vegetation in response to drought stress. *Ecohydrology* 6 (6), 956–973. <https://doi.org/10.1002/eco.1413>.
- Comas, L.H., Becker, S.R., Cruz, V.M.V., Byrne, P.F., Dierig, D.A., 2013. Root traits contributing to plant productivity under drought. *Front. Plant Sci.* 4, 442. <https://doi.org/10.3389/fpls.2013.00442>.
- Dawood, M., 2017. Spatio-statistical analysis of temperature fluctuation using Mann-Kendall and Sen's slope approach. *Clim. Dyn.* 48 (3), 783–797. <https://doi.org/10.1007/s00382-016-3110-y>.
- Deng, W., Chen, M., Zhao, Y., Yan, L., Wang, Y., Zhou, F., 2022. The role of groundwater depth in semiarid grassland restoration to increase the resilience to drought events: a lesson from Horqin Grassland, China. *Ecol. Indic.* 141, 109122. <https://doi.org/10.1016/j.ecolind.2022.109122>.
- Dhital, Y.P., Tang, Q., Shi, J., 2013. Hydroclimatological changes in the Bagmati River basin, Nepal. *J. Geogr. Sci.* 23 (4), 612–626. <https://doi.org/10.1007/s11442-013-1032-8>.
- Ding, Y., Zhang, L., He, Y., Cao, S., Gusev, A., Guo, Y., Ran, L., Wei, X., Mikalai, F., 2024. Nonlinear effects of agricultural drought on vegetation productivity in the Yellow River Basin, China. *Sci. Total Environ.* 948, 174903. <https://doi.org/10.1016/j.scitotenv.2024.174903>.
- Drumond, A., Stojanovic, M., Nieto, R., Gimeno, L., Liberato, M.L., Pauliquevis, T., Ambrizzi, T., 2021. Dry and wet climate periods over Eastern South America: identification and characterization through the SPEI index. *Atmosphere* 12 (2), 155. <https://doi.org/10.3390/atmos12020155>.
- Fang, W., Huang, S., Huang, Q., Huang, G., Wang, H., Leng, G., Wang, L., Guo, Y., 2019. Probabilistic assessment of remote sensing-based terrestrial vegetation vulnerability to drought stress of the Loess Plateau in China. *Rem. Sens. Environ.* 232, 111290. <https://doi.org/10.1016/j.rse.2019.111290>.
- Guo, H., Tian, Y., Li, J., Meng, X., Lv, X., Wang, W., Bao, A., Zhu, L., Nzabarinda, V., De Maeyer, P., 2024. Unveiling the spatiotemporal impacts of the 2021 Central Asian drought on vegetation: a comprehensive quantitative analysis. *Ecol. Indic.* 165, 112238. <https://doi.org/10.1016/j.ecolind.2024.112238>.
- He, Q., Ju, W., Dai, S., He, W., Song, L., Wang, S., Mao, G., 2021. Drought risk of global terrestrial gross primary productivity in recent 40 years detected by a remote sensing-driven process model. *Journal of Geophysical Research-Biogeosciences* 126, e2020JG005944. <https://doi.org/10.1029/2020JG005944>.
- He, Y., Chen, F., Jia, H., Wang, L., Bondur, V.G., 2020. Different drought legacies of rain-fed and irrigated croplands in a typical Russian agricultural region. *Remote Sens.* 12 (11), 1700. <https://doi.org/10.3390/rs12111700>.
- Huang, W., Henderson, M., Liu, B., Su, Y., Zhou, W., Ma, R., Chen, M., Zhang, Z., 2024. Cumulative and lagged effects: seasonal characteristics of drought effects on East Asian grasslands. *Remote Sens.* 16 (18), 3478. <https://doi.org/10.3390/rs16183478>.
- Immerzeel, W.W., Van Beek, L.P., Bierkens, M.F., 2010. Climate change will affect the Asian water towers. *science* 328 (5984), 1382–1385. <https://doi.org/10.1126/science.1183188>.
- Jarvis, P., Rey, A., Petsikos, C., Wingate, L., Rayment, M., Pereira, J., Banza, J., David, J., Miglietta, F., Borghetti, M., Manca, J., Valentini, R., 2007. Drying and wetting of Mediterranean soils stimulates decomposition and carbon dioxide emission: the “Birch effect”. *Tree Physiol.* 27 (7), 929–940. <https://doi.org/10.1093/treephys/27.7.929>.
- Jiang, L., Liu, B., Guo, H., Yuan, Y., Liu, W., Jiapaer, G., 2024. Assessing vegetation resilience and vulnerability to drought events in Central Asia. *J. Hydrol.* 634, 131012. <https://doi.org/10.1016/j.jhydrol.2024.131012>.
- Kendall, M.G., 1948. Rank correlation methods.
- Knapp, A.K., Smith, M.D., 2001. Variation among biomes in temporal dynamics of aboveground primary production. *Science* 291 (5503), 481–484. <https://doi.org/10.1126/science.291.5503.481>.
- Konings, A.G., Saatchi, S.S., Frankenberger, C., Keller, M., Leshyk, V., Anderegg, W.R., Zuidema, P.A., 2021. Detecting forest response to droughts with global observations of vegetation water content. *Glob. Change Biol.* 27 (23), 6005–6024. <https://doi.org/10.1111/gcb.15872>.
- Li, X., Piao, S., Huntingford, C., Peñuelas, J., Yang, H., Xu, H., Chen, A., Friedlingstein, P., Keenan, T.F., Sitch, S., Wang, X., Zscheischler, J., Mahecha, M.D., 2023. Global variations in critical drought thresholds that impact vegetation. *Natl. Sci. Rev.* 10 (5), nwad049. <https://doi.org/10.1093/nsr/nwad049>.
- Li, Y., Yang, J., Wu, J., Zhang, Z., Xia, H., Ma, Z., Gao, L., 2025. Spatiotemporal responses and vulnerability of vegetation to drought in the Ili River transboundary Basin: a comprehensive analysis based on copula theory, SPEI, and NDVI. *Remote Sens.* 17 (5), 801. <https://doi.org/10.3390/rs17050801>.
- Lian, X., Piao, S., Chen, A., Huntingford, C., Fu, B., Li, L.Z., Roderick, M.L., 2021. Multifaceted characteristics of dryland aridity changes in a warming world. *Nat. Rev. Earth Environ.* 2 (4), 232–250. <https://doi.org/10.1038/s43017-021-00144-0>.
- Liang, H., Wang, D., Zheng, J., 2020. Temporal and spatial characteristics of surface evapotranspiration in the Ili River Basin. *Journal of Irrigation and Drainage* 39 (7), 100–110. <https://doi.org/10.13522/j.cnki.ggps.2019415>. In Chinese.
- Lioubimtseva, E., Henebry, G.M., 2009. Climate and environmental change in arid Central Asia: impacts, vulnerability, and adaptations. *J. Arid Environ.* 73 (11), 963–977. <https://doi.org/10.1016/j.jaridenv.2009.04.022>.
- Liu, L., Guan, J., Zheng, J., Wang, Y., Han, W., Liu, Y., 2023a. Cumulative effects of drought have an impact on net primary productivity stability in Central Asian grasslands. *J. Environ. Manag.* 344, 118734. <https://doi.org/10.1016/j.jenvman.2023.118734>.
- Liu, L., Peng, J., Li, G., Guan, J., Han, W., Ju, X., Zheng, J., 2023b. Effects of drought and climate factors on vegetation dynamics in Central Asia from 1982 to 2020. *J. Environ. Manag.* 328, 116997. <https://doi.org/10.1016/j.jenvman.2022.116997>.
- Liu, N., Ding, Y., Peng, S., 2021a. Temporal effects of climate on vegetation trigger the response biases of vegetation to human activities. *Global Ecology and Conservation* 31, e01822. <https://doi.org/10.1016/j.gecco.2021.e01822>.
- Liu, X., Yu, S., Yang, Z., Dong, J., Peng, J., 2024. The first global multi-timescale daily SPEI dataset from 1982 to 2021. *Sci. Data* 11 (1), 223. <https://doi.org/10.1038/s41597-024-03047-z>.
- Liu, Y., Tian, J., Liu, R., Ding, L., 2021b. Influences of climate change and human activities on NDVI changes in China. *Remote Sens.* 13 (21), 4326. <https://doi.org/10.3390/rs13214326>.
- Liu, Y., Zheng, J., Guan, J., Han, W., Liu, L., 2023c. Concurrent and lagged effects of drought on grassland net primary productivity: a case study in Xinjiang, China. *Frontiers in Ecology and Evolution* 11, 1131175. <https://doi.org/10.3389/fevo.2023.1131175>.

- Lozano, Y.M., Aguilar-Trigueros, C.A., Flaig, I.C., Rillig, M.C., 2020. Root trait responses to drought are more heterogeneous than leaf trait responses. *Funct. Ecol.* 34 (11), 2224–2235. <https://doi.org/10.1111/1365-2435.13656>.
- Lu, J., Peng, J., Li, G., Guan, J., Han, W., Liu, L., Zheng, J., 2023. Assessment of time-lag and cumulative effects of drought on gross primary productivity of grassland in Central Asia from 1982 to 2018. *Acta Ecol. Sin.* 43 (23), 9745–9757. <https://doi.org/10.20103/j.stxb.202209162644>. In Chinese.
- Luo, N., Mao, D., Wen, B., Liu, X., 2020. Climate change affected vegetation dynamics in the northern Xinjiang of China: evaluation by SPEI and NDVI. *Land* 9 (3), 90. <https://doi.org/10.3390/land9030090>.
- Mann, H.B., 1945. Nonparametric tests against trend. *Econometrica: J. Econom. Soc.* 245–259. <https://doi.org/10.2307/1907187>.
- Mishra, A.K., Singh, V.P., 2010. A review of drought concepts. *J. Hydrol.* 391 (1–2), 202–216. <https://doi.org/10.1016/j.jhydrol.2010.07.012>.
- Mondal, A., Kundu, S., Mukhopadhyay, A., 2012. Rainfall trend analysis by Mann-Kendall test: a case study of north-eastern part of Cuttack district, Orissa. *International Journal of Geology, Earth and Environmental Sciences* 2 (1), 70–78. <http://www.cibtech.org/jgee.htm>.
- Peng, J., Wu, C., Zhang, X., Wang, X., Gonsamo, A., 2019. Satellite detection of cumulative and lagged effects of drought on autumn leaf senescence over the Northern hemisphere. *Glob. Change Biol.* 25 (6), 2174–2188. <https://doi.org/10.1111/gcb.14627>.
- Schwinning, S., Sala, O.E., 2004. Hierarchy of responses to resource pulses in arid and semi-arid ecosystems. *Oecologia* 141, 211–220. <https://doi.org/10.1007/s00442-004-1520-8>.
- Sen, P.K., 1968. Estimates of the regression coefficient based on Kendall's tau. *J. Am. Stat. Assoc.* 63 (324), 1379–1389. <https://doi.org/10.1080/01621459.1968.10480934>.
- Sheffield, J., Wood, E.F., 2007. Characteristics of global and regional drought, 1950–2000: analysis of soil moisture data from off-line simulation of the terrestrial hydrologic cycle. *J. Geophys. Res. Atmos.* 112 (D17). <https://doi.org/10.1016/j.jhydrol.2024.131012>.
- Sullivan, C.Y., Eastin, J.D., 1975. Plant physiological responses to water stress. *Dev. Agric. Manag. For. Ecol.* 1, 113–127. <https://doi.org/10.1016/B978-0-444-41273-7.50015-5>.
- Theil, H., 1950. A rank-invariant method of linear and polynomial regression analysis. *Indagat. Math.* 12 (85), 173.
- Tirivarombo, S.O.D.E., Osipile, D., Eliasson, P., 2018. Drought monitoring and analysis: standardised precipitation evapotranspiration index (SPEI) and standardised precipitation index (SPI). *Phys. Chem. Earth, Parts A/B/C* 106, 1–10. <https://doi.org/10.1016/j.pce.2018.07.001>.
- van der Molen, M.K., Dolman, A.J., Ciais, P., Eglin, T., Gobron, N., Law, B.E., Wang, G., 2011. Drought and ecosystem carbon cycling. *Agric. For. Meteorol.* 151 (7), 765–773. <https://doi.org/10.1016/j.agrformet.2011.01.018>.
- Wang, Q., Zeng, J., Qi, J., Zhang, X., Zeng, Y., Shui, W., Xu, Z., Zhang, R., Wu, X., Cong, J., 2021. A multi-scale daily SPEI dataset for drought characterization at observation stations over mainland China from 1961 to 2018. *Earth Syst. Sci. Data* 13 (2), 331–341. <https://doi.org/10.5194/essd-13-331-2021>.
- Wei, X., He, W., Zhou, Y., Ju, W., Xiao, J., Li, X., Cheng, N., 2022. Global assessment of lagged and cumulative effects of drought on grassland gross primary production. *Ecol. Indic.* 136, 108646. <https://doi.org/10.1016/j.ecolind.2022.108646>.
- Wen, Y., Liu, X., Xin, Q., Wu, J., Xu, X., Pei, F., Wang, Y., 2019. Cumulative effects of climatic factors on terrestrial vegetation growth. *J. Geophys. Res.: Biogeosciences* 124 (4), 789–806. <https://doi.org/10.1029/2018JG004751>.
- Wilhite, D.A., 2016. Drought as a Natural Hazard: Concepts and Definitions. *Droughts*. Routledge.
- Wu, C., Wang, T., 2022. Evaluating cumulative drought effect on global vegetation photosynthesis using numerous GPP products. *Front. Environ. Sci.* 10, 908875. <https://doi.org/10.3389/fenvs.2022.908875>.
- Wu, X., Zhang, R., Bento, V.A., Leng, S., Qi, J., Zeng, J., Wang, Q., 2022. The effect of drought on vegetation gross primary productivity under different vegetation types across China from 2001 to 2020. *Remote Sens.* 14 (18), 4658. <https://doi.org/10.3390/rs14184658>.
- Xi, H., Xu, B., Huang, F., Yang, Y., Chen, Y., Lu, Z., Qu, L., 2024. Impact causes of runoff in mountainous areas of the Ili River Basin. *Chinese Journal of Nature* 1–10. <http://kns.cnki.net/kcms/detail/31.1418.N.2024016.1411.002.html>. In Chinese.
- Xu, C., McDowell, N.G., Fisher, R.A., Wei, L., Sevanto, S., Christoffersen, B.O., Middleton, R.S., 2019. Increasing impacts of extreme droughts on vegetation productivity under climate change. *Nat. Clim. Change* 9 (12), 948–953. <https://doi.org/10.1038/s41558-019-0630-6>.
- Xu, H.J., Wang, X.P., Zhao, C.Y., 2021. Drought sensitivity of vegetation photosynthesis along the aridity gradient in northern China. *Int. J. Appl. Earth Obs. Geoinf.* 102, 102418. <https://doi.org/10.1016/j.jag.2021.102418>.
- Xu, S., Wang, Y., Liu, Y., Li, J., Qian, K., Yang, X., Ma, X., 2023. Evaluating the cumulative and time-lag effects of vegetation response to drought in Central Asia under changing environments. *J. Hydrol.* 627, 130455. <https://doi.org/10.1016/j.jhydrol.2023.130455>.
- Yang, M., Zou, J., Ding, J., Zou, W., Yahefujiang, H., 2023. Stronger cumulative than lagged effects of drought on vegetation in Central Asia. *Forests* 14 (11), 2142. <https://doi.org/10.3390/f14112142>.
- Yu, T., Jiapaer, G., Bao, A., Yuan, Y., Bao, J., Van de Voorde, T., 2025. Soil moisture dominates gross primary productivity variation during severe droughts in Central Asia. *Ecol. Inform.*, 103076. <https://doi.org/10.1016/j.ecoinf.2025.103076>.
- Yu, T., Jiapaer, G., Long, G., Li, X., Jing, J., Liu, Y., De Maeyer, P., Van de Voorde, T., 2023. Interannual and seasonal relationships between photosynthesis and summer soil moisture in the Ili River basin, Xinjiang, 2000–2018. *Sci. Total Environ.* 856, 159191. <https://doi.org/10.1016/j.scitotenv.2022.159191>.
- Zhang, H., Liu, S., Regnier, P., Yuan, W., 2018a. New insights on plant phenological response to temperature revealed from long-term widespread observations in China. *Glob. Change Biol.* 24 (5), 2066–2078. <https://doi.org/10.1111/gcb.14002>.
- Zhang, R., Wang, Z., Han, G., Schellenberg, M.P., Wu, Q., Gu, C., 2018b. Grazing induced changes in plant diversity is a critical factor controlling grassland productivity in the Desert Steppe, Northern China. *Agric. Ecosyst. Environ.* 265, 73–83. <https://doi.org/10.1016/j.agee.2018.05.014>.
- Zhang, X., Hao, Z., Singh, V.P., Zhang, Y., Feng, S., Xu, Y., Hao, F., 2022a. Drought propagation under global warming: characteristics, approaches, processes, and controlling factors. *Sci. Total Environ.* 838, 156021. <https://doi.org/10.1016/j.scitotenv.2022.156021>.
- Zhang, Z., Ju, W., Zhou, Y., Li, X., 2022b. Revisiting the cumulative effects of drought on global gross primary productivity based on new long-term series data (1982–2018). *Glob. Change Biol.* 28 (11), 3620–3635. <https://doi.org/10.1111/gcb.16178>.
- Zhao, A., Yu, Q., Feng, L., Zhang, A., Pei, T., 2020. Evaluating the cumulative and time-lag effects of drought on grassland vegetation: a case study in the Chinese Loess Plateau. *J. Environ. Manag.* 261, 110214. <https://doi.org/10.1016/j.jenvman.2020.110214>.